

# 1 Aerosol pH Indicator and Organosulfate Detectability from Aerosol Mass Spectrometry

## 2 Measurements

3 Melinda K. Schueneman<sup>1</sup>, Benjamin A. Nault<sup>1,a</sup>, Pedro Campuzano-Jost<sup>1</sup>, Duseong S. Jo<sup>1,2</sup>,  
4 Douglas A. Day<sup>1</sup>, Jason C. Schroder<sup>1,b</sup>, Brett B. Palm<sup>1</sup>, Alma Hodzic<sup>2</sup>, Jack E. Dibb<sup>3</sup>, and Jose L.  
5 Jimenez<sup>1</sup>

6 [1] Department of Chemistry, and Cooperative Institute for Research in Environmental Sciences  
7 (CIRES), University of Colorado, Boulder, CO, USA

8 [2] Atmospheric Chemistry Observations and Modeling, National Center for Atmospheric  
9 Research, Boulder, CO 80301, USA

10 [3] Earth Systems Research Center, Institute for the Study of Earth, Oceans, and Space,  
11 University of New Hampshire, USA

12 a. Now at: Aerodyne Research, Inc., Billerica, MA, USA

13 b. Now at: Air Pollution Control Division, Colorado Department of Public Health and the  
14 Environment, Denver, CO, USA

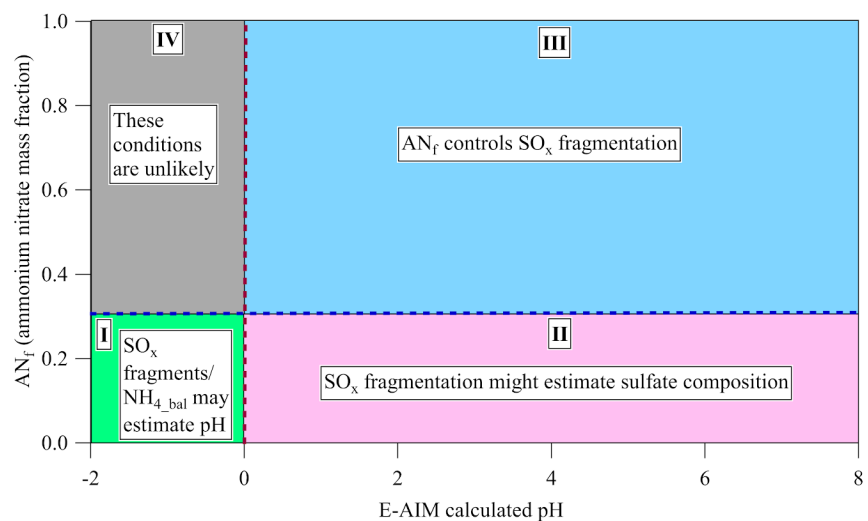
15 Correspondence: jose.jimenez@colorado.edu

## 16 Abstract

17 Aerosol sulfate is a major component of submicron particulate matter ( $PM_{10}$ ). Sulfate can be  
18 present as inorganic (mainly ammonium sulfate, AS) or organosulfate (OS). Although OS is  
19 thought to be a smaller fraction of total sulfate in most cases, recent literature argues that this  
20 may not be the case in more polluted environments. Aerodyne Aerosol Mass Spectrometers  
21 (AMS) measure total submicron sulfate, but it has been difficult to apportion AS vs. OS as the  
22 detected ion fragments are similar. Recently, two new methods have been proposed to quantify  
23 OS separately from AS with AMS data. We use observations collected during several airborne  
24 field campaigns covering a wide range of sources and air mass ages (spanning the continental US,  
25 marine remote troposphere, and Korea) and targeted laboratory experiments to investigate the  
26 performance and validity of the proposed OS methods. Four chemical regimes are defined to  
27 categorize the factors impacting sulfate fragmentation. In polluted areas with high ammonium  
28 nitrate concentrations and in

29 remote areas with high  
30 aerosol acidity, the  
31 decomposition and  
32 fragmentation of sulfate in  
33 the AMS is influenced by  
34 multiple complex effects,  
35 and estimation of OS does  
36 not seem possible with  
37 current methods. In regions  
38 with lower acidity ( $pH > 0$ )  
39 and ammonium nitrate  
40 (fraction of total mass  $< 0.3$ ),  
41 the proposed OS methods  
42 might be more reliable,

43 although application of these methods often produced nonsensical results. However, the  
44 fragmentation of ambient neutralized sulfate varies somewhat within studies, adding uncertainty,  
45 possibly due to variations in the effect of organics. Under highly acidic conditions (when  
46 calculated  $pH < 0$  and ammonium balance  $< 0.65$ ), sulfate fragment ratios show a clear relationship  
47 with acidity. The measured ammonium balance (and to a lesser extent, the  $H_ySO_x^+ / SO_x^+$  AMS  
48 ratio) is a promising indicator for rapid estimation of aerosol  $pH < 0$ , including when gas-phase  
49  $NH_3$  and  $HNO_3$  are not available. These results allow an improved understanding of important  
50 intensive properties of ambient aerosols.



## 51 **Introduction**

52  $PM_{10}$ , or submicron aerosols, have important impacts on visibility, climate, and  
53 environmental and human health (Dockery et al., 1996; Lighty et al., 2000; Lohmann et al.,  
54 2004; IPCC, 2013). In order to quantify the impacts of  $PM_{10}$ , and their evolution with changes in  
55 emissions, chemistry, and climate,  $PM_{10}$  sources, chemistry, and composition must be understood.  
56 Field measurements are critical to that goal, and one tool used extensively in field studies since  
57 the early 2000s is the Aerodyne Aerosol Mass Spectrometer (AMS) and more recently its  
58 simplified version, the Aerosol Chemical Speciation Monitor (ACSM) (Jayne et al., 2000;  
59 DeCarlo et al., 2006; Canagaratna et al., 2007; Ng et al., 2011a). The AMS typically quantifies  
60 the chemical composition and size distribution of sulfate, nitrate, organic aerosol (OA),  
61 ammonium, and chloride (Jayne et al., 2000; DeCarlo et al., 2006; Canagaratna et al., 2007;  
62 Jimenez et al., 2009).

63 Within the AMS, particles are vaporized, leading to some thermal decomposition (e.g.,  
64 Docherty et al., 2015) and then ionized via 70 eV electron ionization, which leads to substantial  
65 fragmentation of the molecular ions. Despite or perhaps because of the substantial (and  
66 reproducible) decomposition and fragmentation, the relative signals of different AMS fragments  
67 have been found to be indicative of different chemical species in the aerosol. These include the  
68 presence of inorganic vs. organic nitrates (Farmer et al., 2010; Fry et al., 2013), and of several  
69 source and composition characteristics of organic aerosols (Alfarra et al., 2004; Zhang et al.,  
70 2004a; Cubison et al., 2011; Ng et al., 2011b; Hu et al., 2015). In contrast to nitrates,  
71 deconvolving inorganic vs. organosulfates (OS, which includes sulfonic acids, when present) is  
72 thought to be more difficult. The fragmentation pattern for one atmospherically relevant OS was

73 similar to those of inorganic sulfates (mainly ammonium-sulfate salts, AS) in an early study, with  
74 minimal C-S-containing fragments (Farmer et al., 2010). Until recently, most studies have shown  
75 that the OS molar fraction ( $OS_f = OS / (AS + OS)$ , calculated using only the sulfate moiety of the  
76 molecules) typically makes a small (~1-10%) contribution to total sulfate in  $PM_1$  (e.g. Tolocka  
77 and Turpin, 2012; Hu et al., 2015; Liao et al., 2015; Riva et al., 2016, 2019). However, for  
78 biogenic areas  $OS_f$  is predicted to increase substantially in the future (Riva et al., 2019). Another  
79 important recent subject of debate is the missing sources of sulfate production in haze events in  
80 China (Wang et al., 2014; Zheng et al., 2014; Li et al., 2017), which some studies have attributed  
81 to a major contribution of OS (e.g., Song et al., 2019). It should be noted that a recent study  
82 reports that OS filter-based measurements in past scientific studies may have substantial  
83 associated positive biases, leading to an overestimate for [OS] (Brüggemann et al., 2020). It is  
84 also important to quantify OS in order to understand the chemistry of aerosol formation and  
85 aging (Surratt et al., 2007, 2008; Song et al., 2019), which impacts the ability to understand how  
86 sulfate may influence various  $PM_1$  properties and processes (e.g., gas uptake, aqueous reactions).  
87 Finally, accurate AS concentrations are needed to quantify the inorganic:organic ratio (to predict  
88 the hygroscopicity of  $PM_1$ , which impacts satellite and model interpretation) and to estimate  
89 aerosol pH and liquid water content from thermodynamic models, as it is currently still not  
90 possible to measure the aerosol pH in the field in-situ (Hennigan et al., 2015; Guo et al., 2016;  
91 Craig et al., 2018; Pye et al., 2019).

92         Recent AMS work has attempted to quantify  $OS_f$  from the measured individual sulfate  
93 ion signals (Chen et al., 2019; Song et al., 2019). The vaporization and ionization of AS and OS  
94 in the AMS produce similar ion fragments that do not contain a carbon atom, the major ones

95 quantified being  $\text{SO}^+$ ,  $\text{SO}_2^+$ ,  $\text{SO}_3^+$ ,  $\text{HSO}_3^+$ , and  $\text{H}_2\text{SO}_4^+$ . These ions were attributed primarily to  
96 inorganic sulfate in earlier AMS analyses (e.g. Jimenez et al. 2003), but were shown to have a  
97 contribution from organosulfates by (Farmer et al., 2010). Note that these are the ions detected in  
98 the AMS (following ionization/decomposition), and not the ions present in the aerosols  
99 (discussed in Sect. 3.3 and shown in Fig. 2C). However, a recent laboratory study with many OS  
100 standards found reproducible differences in the fragmentation of AS vs OS (Chen et al., 2019).  
101 That study proposed a method using the unique AS ion fragments ( $\text{H}_2\text{SO}_4^+$  and  $\text{HSO}_3^+$ ) divided  
102 by the total sulfate signal ( $\text{H}_2\text{SO}_4^+ + \text{HSO}_3^+ + \text{SO}_3^+ + \text{SO}_2^+ + \text{SO}^+$ ) to apportion OS, AS, and  
103 methylsulfonic acid (MSA, an organosulfur compound, but not an organosulfate) in field  
104 datasets. It is important to note that MSA can be directly measured with the (HR-)AMS (Phinney  
105 et al., 2006; Zorn et al., 2008; Huang et al., 2017; Hodshire et al., 2019), so quantification of  
106 MSA with the method in Chen et al. is not necessary. From this method, an average OS mass  
107 concentration ( $C_{\text{OS}}$ ) of  $0.12 \mu\text{g m}^{-3}$  was estimated for the Southern Oxidant and Aerosol Study  
108 (SOAS) ground campaign in rural Alabama (Carlton et al., 2018), with  $\text{OS}_f \sim 4\%$  (Chen et al.,  
109 2019). That estimate is consistent with others for that site and region (Hu et al., 2015; Liao et al.,  
110 2015). An alternative method to estimate  $\text{OS}_f$  based on the same principle was proposed by Song  
111 et al. (2019) using the observed AMS  $\text{SO}^+/\text{H}_y\text{SO}_x^+$  and  $\text{SO}_2^+/\text{H}_y\text{SO}_x^+$ . These authors reported  
112  $\text{OS}_f \sim 17\% \pm 7\%$  (which corresponds to  $[\text{OS}] \sim 5\text{-}10 \mu\text{g m}^{-3}$ ) during winter haze episodes in China.  
113 A recent study (Dovrou et al., 2019) investigated mixtures of sodium sulfate and sodium  
114 hydroxymethanesulfonate (HMS); however, they found that HMS cannot be distinguished from  
115 AMS ions alone, due to the complex ambient aerosol mixture containing organosulfates, and  
116 inorganic sulfates, which all, in part, produce the same sulfate fragments as HMS.

117 Another important and related analytical challenge is online quantification or estimation  
118 of ambient aerosol acidity from real-time measurements, e.g. during field campaigns. So far,  
119 online aerosol pH measurements have only been performed in the laboratory (Rindelaub et al.,  
120 2016; Craig et al., 2018). Aerosol acidity is important because it impacts human health by  
121 decreasing lung function (Raizenne et al., 1996), and strongly impacts the equilibria and kinetics  
122 of a very large number of atmospheric physical and chemical processes (Jang et al., 2002;  
123 Meskhidze et al., 2003; Anon, 2007; Thornton et al., 2008; Bertram and Thornton, 2009; Gaston  
124 et al., 2014; Ackendorf et al., 2017; Guo et al., 2017; Losey et al., 2018). In addition, the  
125 deposition of acidic particles leads to damage to terrestrial and freshwater ecosystems, i.e. “acid  
126 rain” or more properly acid deposition (Schindler, 1988; Johnson et al., 2008). Currently, the  
127 state-of-the art technique to quantify aerosol acidity for field data is to run an inorganic aerosol  
128 thermodynamic model that includes the measured particle and gas inorganic concentrations, as  
129 well as temperature and humidity. The Extended Aerosol Inorganics Model (E-AIM) (Clegg et  
130 al., 1998a, 2003; Wexler and Clegg, 2002) is generally considered as the reference model (Pye et  
131 al., 2019). ISORROPIA-II (Nenes et al., 1999; Fountoukis and Nenes, 2007) is a faster model  
132 utilizing look-up tables to calculate aerosol liquid water content (and thus is frequently used as  
133 part of chemical transport models) at the expense of some accuracy at different RH levels (Pye et  
134 al., 2019). In general, these thermodynamic models are thought to perform best for pH estimation  
135 when gas-phase measurements of  $\text{NH}_3$  and/or  $\text{HNO}_3$  are used in the calculations, and to perform  
136 less well when run only with aerosol measurements (Guo et al., 2015; Hennigan et al., 2015;  
137 Song et al., 2018).

138           There has been an ongoing debate about the potential relationship between the inorganic  
139 cation/anion charge ratio (commonly referred to as “ammonium balance”, see Eq. (4)) and  
140 aerosol acidity. Ammonia gas and its particle phase equivalent (ammonium) are the dominant  
141 bases in the atmosphere (Dentener and Crutzen, 1994). As the most important base in  $PM_{10}$ , a  
142 deficit of  $NH_4^+$  vs. dominant  $PM_{10}$  anions,  $SO_4^{2-}$  and  $NO_3^-$  (Jimenez et al., 2009), is indicative of  
143 the concentration of  $H^+$ , since the particles are (nearly) electrically neutral. Thus, in the absence  
144 of substantial non-volatile cations (e.g.  $Na^+$ ,  $K^+$ ) ammonium balance is an indicator of aerosol  
145 acidity. Ammonium balance has been shown to correlate well with pH under certain conditions,  
146 specifically, when using daily averaged temperature and relative humidity (Zhang et al., 2007a),  
147 but has been criticized as being a poor surrogate of pH under other conditions (Hennigan et al.,  
148 2015). In particular, ammonium balance can be a poor surrogate of pH because changes in T and  
149 RH impact the aerosol liquid water in the diurnal cycle (Zhang et al., 2007a). This is especially  
150 important in the boundary layer where almost all past pH quantification has been carried out  
151 (Pye et al., 2019), compared to the lower diurnal variance of T and RH in the free and upper  
152 troposphere. Many field studies do not include measurements of  $NH_3$  or  $HNO_3$ , two species that  
153 are difficult to measure due to inlet delays caused by strong interactions with surfaces. Both  
154 species are typically present at low concentrations and thus not routinely measured, limiting the  
155 ability to calculate aerosol pH (Hennigan et al., 2015). A more direct estimate of aerosol acidity  
156 using only ambient particle data is highly desirable.

157           Here, we analyze sulfate ion fragment data from laboratory and ambient AMS  
158 observations, spanning multiple aircraft campaigns with a routinely calibrated AMS response to  
159 AS, and across a wide range of chemical and meteorological environments. We use this large

160 dataset to test the applicability of recently published methods to partition AS and OS. We  
161 investigate the feasibility of estimating pH based on AMS data; as well as the regions of  
162 chemical space where the different estimation methods may work. Finally, we provide a physical  
163 interpretation for sulfate fragmentation in the AMS.

## 164 **2 Methods**

### 165 **2.1 Airborne Campaigns**

166 Sulfate fragmentation data was obtained using an Aerodyne High-Resolution  
167 Time-of-Flight Aerosol Mass Spectrometer (AMS) (Aerodyne Research Inc., Billerica, MA,  
168 USA; (DeCarlo et al., 2006)). The ambient data used here are from aircraft observations from the  
169 following campaigns (Table 1): DC3 (Barth et al., 2015), SEAC<sup>4</sup>RS (Toon et al., 2016),  
170 WINTER (Schroder et al., 2018), KORUS-AQ (Nault et al., 2018), and ATom-1 and ATom-2  
171 (Guo et al., 2020; Hodzic et al., 2020). Flight paths for all six campaigns are shown in Fig. S1.  
172 These campaigns span polluted urban, partially polluted biogenic, biomass burning smoke, rural,  
173 and remote regions of the atmosphere. DC3 sampled continental / rural conditions with diffuse  
174 pollution and some biomass burning events. WINTER and KORUS-AQ were airborne  
175 campaigns that focused on urbanized regions (although from different regions and times of year  
176 (Table 1)); therefore, the campaigns had appreciable mass concentrations of ammonium nitrate  
177 due to anthropogenic emissions of NO<sub>x</sub> and the subsequent production of HNO<sub>3</sub> that partitions  
178 into the aerosol with ammonia (Seinfeld and Pandis, 2006). SEAC<sup>4</sup>RS focused on regional  
179 background chemistry of the continental United States, which included impacts from biomass  
180 burning, biogenic, and pollution emissions, and upper tropospheric chemistry impacted by



181 convection. Finally, ATom-1 and ATom-2 sampled the remote Pacific and Atlantic basins with  
182 continuous full vertical profiling, in order to study the composition of the remote marine  
183 atmosphere, impacted by long range transported chemical species and marine emissions, and far  
184 from anthropogenic sources. Not all campaigns are usable for all the analyses in this paper,  
185 depending on the quality and completeness of the data. Table 1 indicates which campaigns were  
186 usable for each analysis.

## 187 **2.2 High-Resolution Time-of-Flight Aerosol Mass Spectrometer**

188         The highly customized University of Colorado-Boulder aircraft AMS was used in all  
189 campaigns and has been described elsewhere (DeCarlo et al., 2008; Dunlea et al., 2009; Nault et  
190 al., 2018; Schroder et al., 2018; Guo et al., 2020), so only details relevant to this study are  
191 summarized here. Ambient air is drawn through a National Center for Atmospheric Research  
192 (NCAR) High-Performance Instrumented Airborne Platform for Environmental Research  
193 Modular Inlet (HIMIL: (Stith et al., 2009)) with a constant standard flow rate of  $9 \text{ L min}^{-1}$ , and  
194 all data is reported at a constant standard temperature ( $T = 273 \text{ K}$ ) and pressure ( $P = 1013 \text{ hPa}$ ).  
195 The sampled air enters a pressure controlled inlet (Bahreini et al., 2008) and is then introduced  
196 into an aerodynamic focusing lens (Liu et al., 1995; Zhang et al., 2004b). Particles then impact  
197 onto an inverted cone porous tungsten “standard” vaporizer, operated at  $\sim 600 \text{ }^\circ\text{C}$  under high  
198 vacuum. The standard vaporizer is used in this study. A “capture vaporizer” has been recently  
199 demonstrated, it leads to more thermal decomposition while still retaining similar (although  
200 noisier) fragment information (Hu et al., 2017a; Zheng et al., 2020), but it is not used here.  
201 Non-refractory species, those that evaporate in less than a few seconds (such as sulfate, nitrate,

202 ammonium, and organic material), are subsequently ionized by 70 eV electrons. Some refractory  
203 and semi-refractory species such as sea-salt, lead and potassium can be detected by the AMS in  
204 some cases (Lee et al., 2010; Salcedo et al., 2010; Ovadnevaite et al., 2012; Hodzic et al., 2020)).  
205 A cryopump reduces background in the ionizer by orders of magnitude during the flights, leading  
206 to low detection limits, in particular for  $\text{NH}_4$ , which is critical for acidity quantification in the  
207 remote troposphere. Data was taken at 1 Hz, but was processed at both 1 Hz and 1 minute  
208 resolution, and the latter product is primarily used here due to higher signal-to-noise ratios. The  
209 one minute datasets were further filtered by removing points where the sulfate signal was below  
210 three times its detection limit. Detection limits were estimated continuously via the methods of  
211 Drewnick et al. (2009), and confirmed with frequent in-flight filter blanks. For the laboratory  
212 studies, everything was kept the same as on the aircraft other than no use of the HIMIL aircraft  
213 inlet. Data was processed and analyzed with the standard Squirrel and PIKA ToF-AMS data  
214 analysis software packages within Igor Pro 7 (Wavemetrics) (DeCarlo et al., 2006; Sueper,  
215 2018).

216         One important parameter for AMS quantification is collection efficiency (CE). CE is the  
217 probability that a particle entering the AMS is detected. It is affected by several particle  
218 properties (Huffman et al., 2005), the most important being particle bounce off the vaporizer  
219 without detection (Middlebrook et al., 2012). Bounce is controlled by particle phase (Quinn et  
220 al., 2006; Matthew et al., 2008), and is estimated for ambient particles based on their ammonium  
221 balance (acidity) and ammonium nitrate content (Middlebrook et al., 2012). This  
222 parameterization performs well for ambient particles (Middlebrook et al., 2012; Hu et al., 2017a,  
223 2020; Guo et al., 2020). Still, potential variability in CE that is not perfectly captured by the

224 parameterization contributes a major fraction of the AMS uncertainty for ambient particle  
225 analysis (Bahreini et al., 2009). Alternative methods to estimate ambient CE for ambient  
226 particles are of interest, we explore a potential alternative method here.

### 227 **2.3 Quantification of OS/AS using Literature Methods**

228 Two methods have been proposed to quantify OS contribution to total sulfate using AMS  
229 sulfate ion fragment fractions. The first method uses different sulfate ions to attribute measured  
230 total sulfate to either OS, AS, or methanesulfonic acid (MSA). Due to the structure of OS, only  
231 non-hydrogenated sulfate ions, i.e.,  $\text{SO}^+$ ,  $\text{SO}_2^+$  and  $\text{SO}_3^+$ , are produced in the AMS for OS. AS  
232 does produce hydrogenated sulfate ions, i.e.,  $\text{H}_2\text{SO}_4^+$  and  $\text{HSO}_3^+$ , as well as the same  
233 non-hydrogenated sulfate ions produced by OS. Chen et al. (2019) proposed a “triangle method”  
234 to estimate these two species and MSA, based on the observed fragments. Note that mineral  
235 sulfates such as sodium sulfate fragment similarly to OS, and thus these methods need to be  
236 interpreted differently in regions with significant submicron mineral sulfates. MSA calibrations  
237 show variability for the fragments (Chen et al., 2019), and were not performed for all the studies  
238 in this work. Since MSA can be quantified without using the sulfate fragments, here we apply  
239 this method to estimate the fractions of OS and AS by using a one dimensional version of the  
240 triangle (i.e. just the hypotenuse connecting pure OS to pure AS). An alternative method is  
241 based on the same assumptions, but uses different equations to quantify the relative  
242 concentration of OS (Song et al., 2019).

243 Both literature methods for deconvolving sulfate as OS and AS assume that the main  
244 factor impacting sulfate fragmentation in the AMS is sulfate structure (OS, AS, or MSA). Chen

245 et al. (2019) briefly mention that acidity can impact sulfate fragmentation, but this effect has not  
 246 been studied and quantified. In addition, Chen et al. (2019) used pure standards to quantify the  
 247 AMS fragmentation of different species, but did not explore potential matrix effects in AMS  
 248 fragments which could impact internally mixed ambient particles.

#### 249 **2.4 Quantification of the AMS Sulfate Fragment Ratios**

250 To compare our field data to that analyzed in Chen et al. (2019) we use the variables  
 251 defined in that study,  $fH_2SO_4^+$  and  $fHSO_3^+$  and define the normalized  $nfH_2SO_4^+$  and  $nfHSO_3^+$   
 252 (normalized to the values of  $fH_2SO_4^+$  and  $fHSO_3^+$  for pure AS) :

$$fH_2SO_4^+ = \frac{[H_2SO_4^+]}{[H_2SO_4^+]+[HSO_3^+]+[SO_3^+]+[SO_2^+]+[SO^+]} \quad \text{Eq. 1}$$

$$nfH_2SO_4^+ = \frac{fH_2SO_4^+}{fH_2SO_4^+(pure\ AS)} \quad \text{Eq. 2}$$

$$fHSO_3^+ = \frac{[HSO_3^+]}{[H_2SO_4^+]+[HSO_3^+]+[SO_3^+]+[SO_2^+]+[SO^+]} \quad \text{Eq. 3}$$

$$nfHSO_3^+ = \frac{fHSO_3^+}{fHSO_3^+(pure\ AS)} \quad \text{Eq. 4}$$

253 It should be noted that while that study includes methanesulfonic acid (MSA) data, the impact of  
 254 MSA on  $fH_2SO_4^+$  and  $fHSO_3^+$  is minimal for the ATom campaigns (see Fig. S2). Additionally,  
 255 one study over the Western United States (representing a rural, continental region) observed  
 256 MSA concentrations of  $\sim 50 \text{ ng m}^{-3}$  (Sorooshian et al., 2015), which results in a very small  
 257 deviation in the Chen triangle and can hence be neglected for the purposes of this work. All

258 variables were normalized to the values of the same variables for pure AS calibrations  
 259 (conducted during each field experiment) in order to eliminate some of the spread in the sulfate  
 260 ions that is likely due to instrument-to-instrument or instrument-in-time variability (Fry et al.,  
 261 2013; Chen et al., 2019) (Fig. S3) . We also define a new AMS sulfate ion ratio,  $H_ySO_x^+/SO_x^+$ ,  
 262 and create the normalized  $nH_ySO_x^+/SO_x^+$  to reduce the influence of instrument-to-instrument or  
 263 instrument-in-time variability:

$$H_ySO_x^+/SO_x^+ = \frac{[H_ySO_x^+]}{[SO_x^+]} = \frac{[H_2SO_4^+]+[HSO_3^+]}{[SO_3^-]+[SO_2^-]+[SO^-]} \quad \text{Eq. 5}$$

$$nH_ySO_x^+/SO_x^+ = \frac{H_ySO_x^+/SO_x^+}{H_ySO_x^+/SO_x^+ \text{ (pure AS)}} \quad \text{Eq. 6}$$

264 The submicron aerosol molar Ammonium Balance ( $NH_{4\_bal}$ ) is calculated as:

$$NH_{4\_bal} = \frac{[NH_4]/18}{([SO_4]/48)+([NO_3]/62)+([Chl]/35)} \quad \text{Eq. 7}$$

265 The concentration of non-refractory chloride is only included for non-remote campaigns  
 266 (KORUS-AQ, WINTER, and SEAC<sup>4</sup>RS), since it was negligible for others and strongly  
 267 impacted by seasalt in the marine boundary layer. The fraction of ammonium nitrate in the  
 268 particle phase (ammonium nitrate mass fraction,  $AN_p$ ) (by mass):

$$AN_f = \frac{(80+62) \times [Inorganic NO_3]}{[NO_3]+[SO_4]+[NH_4]+[Chl]+[Org]} \quad \text{Eq. 8}$$

269 The fraction of total AMS aerosol mass comprised of OA ( $OA_f$ ) is:

$$OA_f = \frac{[Org]}{[NO_3]+[SO_4]+[NH_4]+[Chl]+[Org]} \quad \text{Eq. 9}$$

270 The sulfate equivalent concentration of OS in the Song et al. (2019) paper is calculated as:

$$C_{OS} = M_{SO_4^{2-}} \left[ \frac{SO_{cd, SO^+/H_y SO_x^{+,*}}^{obs-R} \cdot H_y SO_{x, obs}^{+,*}}{M_{SO^+}} + \frac{SO_{cd, SO_2^+/H_y SO_x^{+,*}}^{obs-R} \cdot H_y SO_{x, obs}^{+,*}}{M_{SO_2^+}} \right] \quad \text{Eq. 10}$$

271 where “cd” stands for “clean and dry”. Clean and dry conditions are defined in Song et al. (2019)  
 272 as ambient data points where  $PM_1 = 10 \mu\text{g m}^{-3}$  and  $RH = 30\%$ . Clean and dry conditions are  
 273 assumed to represent nearly pure AS. M is for the molar mass of the different sulfate ions, and  
 274 “obs” represents the ambient data for specific sulfate fragments.  $H_y SO_x^{+,*}$  (which differs from the  
 275 notation used in Song’s paper, but is necessary to differentiate  $H_y SO_x^+$  between the Chen and  
 276 Song papers) is defined in Song et al. (2019) as  $(SO_3^+ + HSO_3^+ + H_2SO_4^+)$ . For the Chen method,  
 277 the  $C_{OS}$  is defined based on the AS normalized  $nfH_2SO_4^+$  values:

$$C_{OS} = [SO_4] - nfH_2SO_4^+ * [SO_4] \quad \text{Eq. 11}$$

278  $OS_f$ , the fraction of OS:total sulfate is defined as:

$$OS_f = \frac{C_{OS}}{[SO_4]} \quad \text{Eq. 12}$$

279 Where  $C_{OS}$  is calculated from Eq. (10) or Eq. (11).

## 280 2.5 Laboratory Experiments

281 As ambient aerosols contain mixtures of chemical species, we investigated if matrix  
 282 effects may impact the fragmentation of sulfate species. Different solution mixtures, composed  
 283 of various amounts of AS (Certified ACS, 99.7% purity) and ammonium nitrate (AN) (Certified  
 284 ACS, 99.9% purity) in water (Milli-Q grade ( $R > 19 \text{ MOhms}$ )) were atomized to generate  
 285 particles and size selected using a Differential Mobility Analyzer (DMA) (TSI Model 3081),  
 286 analyzed with a Condensation Particle Counter (CPC) (Model 3775), and electrostatic classifier

287 (Model 3080), for mobility diameters between 350-400 nm. We investigated AS/AN mixtures,  
288 ranging from  $AN_f = 0\%$  to 95%.

289 In order to assess effects on the sulfate fragmentation from mixing with OA, chamber  
290 experiments, where different types of SOA were formed by gas-phase reactions and  
291 condensation onto AS seeds, were investigated. SOA was formed from alkanol and toluene  
292 photooxidation under high- $NO_x$  conditions (Liu et al., 2019), as well as  $\Delta$ -3-carene and  $\alpha$ -pinene  
293 reactions with nitrate radicals Kang et al. (2016). Experiments were initiated with 100% AS in a  
294 dry chamber ( $RH < 5\%$ ;  $\sim 298$  K) followed by either rapid, gradual, or stepwise increases of  
295 SOA until a maximum OA/(OA+AS) ratio of  $\sim 70\%$  was reached. Aerosol composition was  
296 monitored by AMS and size distributions were monitored with a scanning mobility particle sizer  
297 (SMPS: DMA was TSI Model 3081, electrostatic classifier was Model 3080, and the CPC was  
298 Model 3775). RIE of sulfate was directly calibrated with pure ammonium sulfate, while RIE \*  
299 CE of the SOA produced was estimated by comparison to the SMPS integrated volume, together  
300 with OA density estimated from the AMS-derived elemental ratios per Kuwata et al. (2012)), in  
301 order to accurately quantify OA/(OA+AS). Humid experiments were not considered here due to  
302 the potential of forming organosulfates.

## 303 **2.6 E-AIM Thermodynamic Model for pH Estimation**

304 Aerosol pH was estimated using the Extended Aerosol Inorganic Model (E-AIM) Model  
305 IV (Clegg et al., 1998b; Massucci et al., 1999; Wexler and Clegg, 2002). We input into the model  
306 (ran in “forward mode”), the total nitrate (gas-phase  $HNO_3$  plus particle-phase total  $NO_3^-$ ),  
307 sulfate, ammonium, relative humidity (calculated according to the parameterization of Murphy

308 and Koop (2005), which is critical for upper tropospheric conditions), and temperature. Total  
309 nitrate (inorganic+organic) was input, as Nault et al. (2021) found that removing estimated  
310 organic nitrate does not impact the pH calculation. This was done to calculate aerosol liquid  
311 water and aerosol pH. Model IV was not run with chloride ions, as their concentrations were  
312 very low, and including chloride limits the model to temperatures  $\geq 263$  K (Friese and Ebel,  
313 2010), which would greatly limit the analysis of calculated pH for WINTER, ATom-1, and  
314 ATom-2. We have added the modifier “calculated” before pH for all situations where we are  
315 describing the E-AIM pH, and “estimated” when we refer to pH from the empirical estimation  
316 methods from AMS measurements, introduced in this study. Also, including chloride precludes  
317 running the model under supersaturated solution conditions, which is a closer approximation of  
318 ambient aerosol (Pye et al., 2019). All aerosol mass concentrations were from the CU AMS.  
319  $\text{HNO}_3(\text{g})$  was measured by the California Institute of Technology chemical ionization mass  
320 spectrometer (CIT-CIMS) (Crouse et al., 2006), which was flown in all of these missions  
321 (excluding WINTER, where the UW-CIMS was used for the  $\text{HNO}_3$  measurements) (Lee et al.,  
322 2014, 2018). Results are generally similar when using the SAGA mist chamber measurement for  
323 total nitrate (Nault et al., 2020). The forward mode is less sensitive to uncertainties in  
324 measurements than the “reverse mode,” which only uses particle composition and T/RH as  
325 inputs (Hennigan et al., 2015). Also, due to lack of  $\text{NH}_3(\text{g})$  measurements, the model was run  
326 iteratively until convergence in modeled  $\text{NH}_3$  occurred, similar to Guo et al. (2016). Performance  
327 for calculated pH was investigated by comparing model-calculated  $\text{HNO}_3$  and  $\text{NO}_3^-$  to  
328 measurements, as the partitioning of nitrate between gas- and particle-phase is sensitive to  
329 calculated pH under acidic conditions (Guo et al., 2016). For all campaigns included herein



330 (DC3, WINTER, SEAC<sup>4</sup>RS, KORUS-AQ, ATom-1, and ATom-2), the slopes of HNO<sub>3</sub>  
331 (measured vs. predicted) are within the uncertainty of the measurements; with good correlations  
332 (SI Fig. S4). For NO<sub>3</sub><sup>-</sup>, the slopes are within the measurement uncertainty for five of the six  
333 campaigns. For ATom-2, the NO<sub>3</sub><sup>-</sup> slopes were low; however, for this campaign, the measured  
334 NO<sub>3</sub><sup>-</sup> mass concentrations were extremely low (mean = 0.02 μg sm<sup>-3</sup>), and the calculated pH was  
335 also very low (mean = - 0.5), leading to very little NO<sub>3</sub><sup>-</sup> in the aerosol phase (see SI Fig. S4).

336 In addition, other bases present in the atmosphere (such as amines) were examined. Prior  
337 studies have shown that amines were less than a maximum concentration of 30 ng m<sup>-3</sup> at the  
338 ocean surface (Gibb et al., 1999; Facchini et al., 2008; Müller et al., 2009; Frossard et al., 2014;  
339 van Pinxteren et al., 2015; Youn et al., 2015). Another study by Sorooshian et al., (2009) found  
340 that amine mass concentration dropped off quickly with altitude to concentrations less than 25 ng  
341 m<sup>-3</sup> at an altitude between 200 and 300 m, which is the approximate minimum altitude flown on  
342 the DC-8 during the ATom campaigns. As the one minute detection limit for the AMS data for  
343 amines is typically 10 ng m<sup>-3</sup>, we expect the amine signal to generally be below the limit of  
344 detection, and thus outside of our quantification capabilities. This was observed for AMS data  
345 from the ATom campaigns, using characteristic ions identified in past studies (Murphy et al.,  
346 2007; Ge et al., 2014). It was found that amine ions cannot be distinguished from background for  
347 many ATom flights. Only during one flight in ATom-1, we observed an amine signal (C<sub>2</sub>H<sub>6</sub>N<sup>+</sup>  
348 *m/z* = 44) above the background (see SI Fig. S5). During this flight, amines (from the  
349 contribution of CH<sub>4</sub>N, C<sub>2</sub>H<sub>6</sub>N, and C<sub>3</sub>H<sub>8</sub>N) only accounted for 0.7 ng m<sup>-3</sup> of aerosol, whereas  
350 ammonium accounted for 19 ng m<sup>-3</sup>. Amines can produce the same fragments as ammonium, but  
351 this is only the case for a few percent of the amine fragments (Ge et al., 2014). In this case, the

352 ammonium concentration is 25 times that of the amines. Since amines were even lower during  
353 other flights, we assume the effect of amines to the pH calculation is very small and can be  
354 ignored for E-AIM calculations.

## 355 **2.7 GEOS-Chem Model**

356 We used a global chemical transport model (GEOS-Chem 12.6.1,  
357 doi:10.5281/zenodo.3520966; (Bey et al., 2001)) to investigate modeled global distributions of  
358 ammonium nitrate mass fraction ( $\text{AN}_p$ ) and calculated aerosol pH across different regions.  
359 GEOS-Chem was driven by assimilated meteorological fields from the Modern-Era  
360 Retrospective analysis for Research and Applications version 2 (MERRA2) (Gelaro et al., 2017)  
361 for the year of 2010. The simulation was conducted at  $2^\circ$  (latitude)  $\times$  2.5 (longitude) with 47  
362 vertical layers up to 0.01 hPa and  $\sim$ 30 layers under 200 hPa. We used the Community Emissions  
363 Data System (CEDS) inventory for global anthropogenic emissions (Hoesly et al., 2018) and the  
364 global fire emissions database version 4 (GFED4) for biomass burning emissions (Giglio et al.,  
365 2013). Aerosol pH and gas-particle partitioning of inorganic aerosols were calculated online  
366 using the ISORROPIA-II model within GEOS-Chem (Fountoukis and Nenes, 2007; Pye et al.,  
367 2009). Similar to Jo et al., (2019) sea salt aerosol was excluded from pH calculations based on a  
368 better agreement with the observationally-constrained calculated pH values as suggested by  
369 Nault et al. (2020). Oceanic  $\text{NH}_x$  emissions were also included in this model based on recent  
370 work (Paulot et al., 2015; Nault et al., 2020).

## 371 **3 Results and Discussion**

### 372 3.1 Lab quantification of AMS data

373 Application of the one dimensional Chen method to laboratory data is shown in Fig. 1.  
374 Data are expected to lie inside the triangular region, and be apportioned depending on the  
375 relative distance to the three vertices. For example, data lying at [0.5,0.5] on the line between the  
376 OS and AS points would represent a sample with ~50% OS and ~50% AS. If data clusters  
377 around the [1,1] point where pure AS resides, all of the sulfate is attributed to AS. From applying  
378 this method, it is clear that none of the campaign averages or laboratory data falls between the  
379 [0,0] and [1,1] points, suggesting that there may be additional factors (other than sulfate  
380 composition) impacting the location of data in this triangular region.

381 The effect of internally mixed ammonium nitrate (AN) is shown in Fig. 1A. For mixtures  
382 containing  $AN_f < 50\%$ , data centers around the pure AS point in the Chen triangle. When  $AN_f$  is  
383 increased past 0.50, there is an increase in both  $nhH_ySO_x^+$  ions, even when all of the particulate  
384 sulfate is inorganic. As the particle  $AN_f$  increases up to  $AN_f=0.95$ , the  $OS_f$  estimation becomes  
385 increasingly inaccurate. The method may estimate  $OS_f=0\%$  in the latter situation, when  $OS_f$  is  
386 actually 50%. While  $OS_f=0\%$  may be reasonable in some parts of the atmosphere, and one may  
387 be inclined to accept this result as it is non-negative, it is actually incorrect due to the effect of  
388 particulate AN. Thus for laboratory data, the Chen method should not be used on mixtures  
389 containing  $AN_f > 0.50$ .

390 The effect of OA internally mixed with AS on the sulfate fragmentation pattern was also  
391 explored with toluene, alkanol, and monoterpene SOA (Fig. 1B and Fig. S6). For the alkanol  
392 SOA experiments we found that the presence of even a small coating of alkanol SOA (which is  
393 thought to be liquid (Liu et al., 2019)) shifts the normalized AS [1,1] point to  $\sim[1.08,1.08]$ , but

394 increases in the fraction of OA ( $OA_f$ ) from 0.1 to 0.3 lead to no further changes in  $\eta fH_ySO_x^+$  (Fig.  
395 1B). This means that for a sample containing a mixture of AS and alkanol SOA, the calculated  
396  $OS_f$  would be -15% (Chen). In contrast, toluene SOA, which spans  $0 < OA_f < 0.5$ , shows no  
397 clear change in the  $\eta fH_ySO_x^+$  ions, indicating that  $OA_f$  would not bias the Chen method for this  
398 example. The monoterpene SOA, from two different experimental datasets (2014 and 2015)  
399 using different AMSs, show more varied results than the previous two studies. Overall, the 2014  
400 data shows a very small increase in the “pure” AS value in the  $OA_f$  range 0-0.50, whereas the  
401 2015 monoterpene data shows a consistent and constant 10-20% increase in  $\eta fH_ySO_x^+$  compared  
402 to the pure AS calibration point (similarly to the alkanol SOA). However, when  $OA_f$  is in the  
403 range of  $0.50 < OA_f < 0.70$ , 30-40% increases are observed for the 2014 and 2015 data. This result  
404 is only applicable to a few of the experiments (see Fig. S6), potentially due to very high SOA  
405 loadings (up to  $300 \mu\text{g m}^{-3}$ ). These high OA concentrations could potentially lead to a change of  
406 the particle phase due to condensation of more volatile and liquid species, potentially altering the  
407 interactions of the particles and the vaporizer surfaces. These experiments collectively suggest  
408 that a “pure” AS calibration point of [1.15,1.15] may be more appropriate when applying the  
409 Chen et al. method to some mixed aerosol at typical OA concentrations observed in the  
410 atmosphere; this is discussed further in Sect. 3.2.

411         Chen et al. briefly discussed the potential impact of acidity on their OS quantification  
412 method. This is explored here with pure sulfuric acid lab calibrations (Fig. 1C). Pure sulfuric  
413 acid shows a large deviation from the pure AS triangle point (similar to increasing  $AN_f$ ), nearly  
414 doubling the values for the  $\eta fH_ySO_x^+$  ions. This implies that a particle containing sulfuric acid  
415 would produce a strong negative bias on the estimate of OS by the Chen method.

### 416 3.2 Evaluation of the Chen Method with Aircraft Field studies

417 The results of applying the Chen et al. (2019) method to five aircraft campaigns are  
418 shown in Fig. 1. The effect of internally mixed ammonium nitrate (AN) was explored in Fig. 1A  
419 and Sect. 3.1 (for laboratory studies). Here we explore the effect for field data from KORUS-AQ  
420 (near Seoul, South Korea) where AN was often a major aerosol component; average  $AN_f \sim 0.18$ ).  
421 As discussed in Sect. 3.1, as the percent of AN in laboratory mixtures of AS/AN increases, so do  
422 the  $nfH_ySO_x^+$  ions. The same effect is observed for the KORUS-AQ campaign, although the  
423 departure from the AS vertex is observed at substantially lower AN fractions for the field data  
424 ( $AN_f \sim 0.30$ ). When field data is affected by AN, the Chen method might be applicable for  
425 situations with  $AN_f < 0.30$ . At higher fractions, a correction could potentially be developed, but  
426 with increased resulting uncertainty.

427 The effect of OA (shown in Fig. 1B for laboratory data) on sulfate fragmentation in  
428 ambient data is less clear due to the lack of data that has a lower  $AN_f$ , higher pH, and little/no OS  
429 (see Table S1 for average campaign  $OA_f$ ). In the presence of any one of those factors, the sulfate  
430 fragmentation will be affected. It is especially challenging to confirm the absence of OS, due to  
431 the lack of direct total OS measurements available. In Fig. S7, we isolate a subset of the  
432 KORUS-AQ dataset (where  $AN_f < 0.3$  and  $pH > 0$ , defined as “regime II” and discussed in detail in  
433 Sect. 3.4) to see if there is an offset in the AS under these chemical conditions as observed in the  
434 laboratory data shown in Fig. 1B. Similarly to the lab data, there appears to be a  $\sim 10\%$  offset  
435 between the pure AS  $fH_ySO_x^+$  values from calibrations, and the KORUS-AQ data that occupies  
436 regime II (average  $OA_f \sim 43\%$ ). This offset is smaller than some of the offsets observed in the

437 laboratory data (Fig. 1B and S6), but may hinder the ability of the Chen  $OS_f$  quantification  
438 method to estimate [OS] even in conditions where the  $pH > 0$  and the  $AN_f < 0.3$ .

439 In Fig. 1D, average values for each campaign in regime I, defined as  $AN_f < 0.3$  and  
440 calculated  $pH > 0$ , are shown. For less acidic aerosols/conditions and in the absence of OS or  
441  $AN_f$  effects, it is expected that the data would fall on top of the [1,1] pure AS point in the 1D  
442 triangle plot, but this is not observed. This shift suggests that there are other factors (such as the  
443 presence of organics) that affect the location of the pure AS point. In addition, the average values  
444 for the different campaigns vary substantially, so it is unlikely that a “corrected” pure AS point  
445 can be used for all campaign and/or lab data.

446 To further look into the potential effect of acidity, we consider the ATom campaigns in  
447 Fig. 1C. ATom focused on remote oceanic air, with very low  $AN_f (< 0.01)$ . This is expected as  
448 AN is semivolatile (DeCarlo et al., 2008; Hennigan et al., 2008; Nault et al., 2018) and for the  
449 very low calculated pH conditions during ATom ( $\sim -1$  to  $1$ , average of  $-0.6$ ), most of the nitrate  
450 will be in the form of  $HNO_3(g)$  (Guo et al., 2016). The PALMS instrument independently reports  
451  $OS_f \sim 0.3 - 0.7\%$  for ATom (depending on the pH). The results for ATom span the range between  
452 pure AS and pure  $H_2SO_4$ , following a monotonic trend as acidity increases, consistent with the  
453 laboratory results and the results from the WINTER campaign in Chen et al. (2019). We  
454 hypothesize that high acidity is leading to the observed departure from the Chen triangle. Hence,  
455 the ATom results suggest that all of the sulfate sampled is inorganic and if the Chen method is  
456 applied  $OS_f = -26\%$  to  $+4\%$ . Thus the Chen method is insufficient to describe the trends  
457 observed for very acidic aerosols, until calculated pH increases to  $\sim 0$  (where the ATom data

458 starts to converge onto the pure AS data point). For campaigns containing particles of calculated  
459  $\text{pH} > 0$ , the Chen method might be applicable.

460 To further illustrate that the ATom and KORUS-AQ campaigns are representative of the  
461 range of airmasses in the troposphere, Fig. 1D shows results for two additional campaigns that  
462 focused on the continental US. SEAC<sup>4</sup>RS and WINTER represent chemical regimes that are not  
463 extremely acidic (average calculated  $\text{pH}$  SEAC<sup>4</sup>RS  $\sim -0.2$ , WINTER calculated  $\text{pH} \sim 1.2$ ).  
464 SEAC<sup>4</sup>RS had low  $\text{AN}_f$  ( $\sim 0.04$ ), while WINTER had high  $\text{AN}_f$  ( $\sim 0.25$ ). It is observed that  
465 every single campaign average falls outside of the triangle (for the full campaign and non-acidic,  
466 low  $\text{AN}_f$  averages), indicating that the Chen et al.(2019) method, as proposed, is not applicable to  
467 many regions of the atmosphere. Average  $\text{AN}_p$ ,  $\text{OA}_p$ , and calculated  $\text{pH}$  values for different  
468 campaigns are shown in table S1.

### 469 **3.3 Physical Interpretation of the Sulfate Fragmentation Trends**

470 We note that this section (3.3) should be of most interest for AMS/ACSM users, and can  
471 probably be skipped by others. It is useful to provide a physical interpretation of the trends that  
472 are likely driving the observed sulfate fragmentation changes, based on the physicochemical  
473 details of the AMS detection and those of the particles being sampled. In Fig. 2A, a simplified  
474 diagram of the AMS detection process is shown, highlighting important details that are thought  
475 to give rise to the observed trends.

476 Ambient particles containing AS, OS, and other species are sampled into the AMS  
477 through a focusing lens. Following a series of differential pumping steps through the instrument,  
478 the particles impact on a porous tungsten standard vaporizer. The time spent under vacuum from

479 sampling to detection is of the order of 15 ms. A fraction of the more viscous particles may  
480 bounce from the vaporizer without detection. Non-refractory species in the particles that stick to  
481 the vaporizer (such as OS and AS) are heated by heat transfer from the vaporizer surface. Some  
482 species may evaporate in the form in which they are present in the particle, while others may  
483 thermally decompose to other species, which then evaporate. For example, ammonium sulfate  
484 may evaporate to  $\text{H}_2\text{SO}_4(\text{g})$  and  $\text{NH}_3(\text{g})$ , but it may also thermally decompose to  $\text{SO}_2(\text{g})$ ,  $\text{SO}_3(\text{g})$   
485 and  $\text{H}_2\text{O}(\text{g})$  (Hu et al., 2017b). Finally, these gaseous thermal decomposition products undergo  
486 electron ionization to become positively charged species. Since the electrons used in EI have far  
487 more energy (70 eV) than typical bonds in a molecule ( $\sim 6$  eV for  $\text{S}=\text{O}$ ), the initial ions may  
488 fragment into smaller ions if the ionization process results in absorption of  $> 6$  eV of internal  
489 energy by the molecule, beyond the ionization energy (Lambert, 1998). Some of the evaporated  
490  $\text{H}_2\text{SO}_4(\text{g})$  may remain as  $\text{H}_2\text{SO}_4^+$  after ionization, or it may fragment to  $\text{HSO}_3^+$  or  $\text{SO}_x^+$  ions.  
491  $\text{SO}_2(\text{g})$  can only produce  $\text{SO}_x^+$  ions. Thus the mixture of fragments observed will retain some  
492 memory of the species that evaporated from the particles. If the mixture of evaporating species is  
493 influenced by the particle composition (e.g. pH, AN, OA, or  $\text{OS}_f$ ) then it may be possible to  
494 calibrate the observed relationship to estimate a particle intensive chemical property.

495 Fig. 2A also shows a schematic close-up of the SV surface, which is the main point in the  
496 instrument that controls ammonium sulfate fragmentation. In this diagram, we show a  
497 non-smooth surface with pores, consistent with the fabrication of the vaporizer by sintering 50  
498  $\mu\text{m}$  tungsten spheres. The interaction of a particle with this porous surface is dependent on the  
499 particle phase / viscosity. The red particles represent rigid (more solid-like) particles. These rigid  
500 particles can simply bounce off of the vaporizer, leading to no detection. AS-dominated particles



501 are likely to be rigid (due to the solid phase of pure AS), thus increasing bounce and lowering the  
502 AMS CE (Matthew et al., 2008; Middlebrook et al., 2012). AS particles can also become trapped  
503 in the porous surface. When trapped, they are heated by conduction from the vaporizer surface  
504 and by radiation from surrounding surfaces. They reach higher temperatures that lead to more  
505 thermal decomposition, and a lower  $\text{H}_2\text{SO}_4(\text{g})/\text{SO}_x(\text{g})$  ratio. Consistent with this interpretation, it  
506 was shown that the  $\text{H}_2\text{SO}_4^+/\text{SO}^+$  fragment ratio increased as the vaporizer temperature was  
507 reduced while sampling ambient air, while the  $\text{SO}_2^+/\text{SO}^+$  ratio did not change (Docherty et al.  
508 (2015), their figure S5). In addition, molecules that evaporate as  $\text{H}_2\text{SO}_4(\text{g})$  from these trapped  
509 particles are likely to collide with tungsten surfaces on their way out to the ionization region,  
510 leading to additional thermal decomposition (Hu et al., 2017b) and further reducing the  
511  $\text{H}_2\text{SO}_4(\text{g})/\text{SO}_x(\text{g})$  ratio for the gases reaching the EI region, and thus the  $\text{H}_y\text{SO}_x^+/\text{SO}_x^+$  ion ratio.

512         The second case (blue particle) represents the situation where the particle is less  
513 rigid/viscous or liquid. Acidic sulfate particles (with a lower fraction of the sulfate ions  
514 neutralized by  $\text{NH}_4^+$ ), particles with high  $\text{AN}_p$ , or particles coated with a large water or liquid  
515 organic layer are more likely to deform upon impact and not bounce. This leads to an increased  
516 CE (Matthew et al., 2008; Middlebrook et al., 2012; Hu et al., 2017a). There are several effects  
517 that will lead to a higher  $\text{H}_2\text{SO}_4(\text{g})/\text{SO}_x(\text{g})$  ratio reaching the ionization region in this situation:  
518 (a) evaporated  $\text{H}_2\text{SO}_4(\text{g})$  from particles that impact the front of the vaporizer and do not bounce  
519 can now escape without further collisions with the tungsten surface; (b) the increased surface  
520 area from impact deformation and the lower viscosity allow more  $\text{H}_2\text{SO}_4(\text{g})$  molecules to escape  
521 the particle before those molecules are heated to temperatures that would lead to thermal  
522 decomposition.

523 In Fig. 2B, we show a conceptual model of the impact of these phenomena on the Chen  
524 triangle. For very acidic sulfate (approx. a calculated  $\text{pH} < 0$ ), the liquid character of the  
525 particles leads to less bounce in the vaporizer. It also leads to faster evaporation, which reduces  
526 the internal temperature for the particles and that of the evaporated molecules, leading to less  
527 fragmentation. In this part of the atmosphere,  $\text{OS}_f$  cannot be estimated, but pH may be, as long as  
528 it can be assumed (or shown by additional measurements from the AMS or other instruments)  
529 that  $\text{OS}_f$  and non-volatile cations are small. As an air mass becomes more neutralized by  $\text{NH}_4^+$ ,  
530 the particles become less acidic and more rigid/viscous, leading to more thermal decomposition  
531 of the evaporated species, and the fragmentation of ammonium sulfate occurs at the upper vertex  
532 of the triangle. In this part of the atmosphere, methods such as Chen et al. (2019) may be  
533 applicable to estimate  $\text{OS}_p$ , as long as there are no other effects that interfere with the sulfate  
534 fragments detected (such as substantial non-volatile cations or variations in possible OA effects).  
535 As more ammonia is added to an airmass, the acidity of the particles decreases and the higher pH  
536 favors the partitioning of  $\text{HNO}_3(\text{g})$  to the particle phase, forming ammonium nitrate. If  $\text{AN}_f$   
537 becomes high enough ( $> 0.3$ ), the particles again become less rigid/viscous and the  
538 fragmentation shifts again outside the Chen triangle for the same reasons discussed for the acidic  
539 particles. Finally, Fig. 2C shows the differences in the detection process and the fragments  
540 produced in the AMS for OS and/or AS/ $\text{H}_2\text{SO}_4$ .

### 541 **3.4 Specification of aerosol chemical regimes for feasibility of $\text{OS}_f$ quantification**

542 In Fig. 3A, we introduce a plot of  $\text{AN}_f$  vs. calculated pH that can be used to evaluate the  
543 applicability of the  $\text{OS}_f$  methods to different datasets. Data for five different campaigns (those

544 with AS calibrations, labelled “C” in Table 1) are shown, along with the campaign averages.  
545 Regime I (“highly acidic, low AN<sub>f</sub>”) occupies the bottom left quadrant, where AN<sub>f</sub> < 0.3 and  
546 calculated pH < 0. Campaigns sampling the more remote atmosphere (e.g. ATom-1, 89% of  
547 datapoints; ATom-2, 80%), and a fraction of the data from continental campaigns (SEAC<sup>4</sup>RS,  
548 13% ; DC3 , 40%) fall in this regime. For remote regions, emissions (such as NH<sub>3</sub> and NO<sub>x</sub>) are  
549 generally low. Remote oceanic regions are relatively isolated from the major continental  
550 ammonia sources (Paulot et al., 2015). Therefore, less ammonia is available to balance the  
551 hydronium ions from H<sub>2</sub>SO<sub>4</sub>, leading to high acidity (Quinn et al., 1988; Keene, 2002; Nault et  
552 al., 2020). Highly acidic aerosols and lack of NH<sub>3</sub> shift HNO<sub>3</sub> to the gas phase, so low AN<sub>f</sub> is  
553 observed. In contrast, for sampling in polluted source regions with strong HNO<sub>3</sub> formation and  
554 substantial NH<sub>3</sub> emissions, a much smaller fraction of the data falls in this regime (e.g. only 4%  
555 for KORUS-AQ). In Sect. 3.5 we discuss the potential to estimate pH from AMS data in regime  
556 I.

557 Regime II (lower right) involves less acidic conditions (calculated pH > 0) and lower AN<sub>f</sub>  
558 (< 0.3). In this region sulfate fragmentation in the AMS is not strongly impacted by either AN<sub>f</sub> or  
559 acidity. In principle, in this regime the recently proposed sulfate deconvolution methods could be  
560 applicable. The geographical regions studied in Chen et al. (2019) and Song et al. (2019)  
561 generally fall in this regime, and this might explain the lack of large negative OS<sub>f</sub> values in those  
562 studies, in contrast to our observations for other regions. About half of our campaign data is  
563 located in this regime, more so for the continental campaigns and much less so for the remote  
564 campaigns. Specifically, 65% of KORUS-AQ, 60% of DC3, 87% of SEAC<sup>4</sup>RS, 11% of ATom-1  
565 and 20% of ATom-2 fall in this regime. We have applied the 1D version of the Chen method to

566 each field campaign after filtering it by the  $AN_f$  and calculated pH constraints for regime II.  $OS_f$   
567 is nominally slightly greater than zero for ATom-1,  $OS_f \sim 3\%$ , of the order of the 0.3% estimate  
568 in regime II from PALMS (for ATom-1 and ATom-2, estimated by only considering the sulfate  
569 moiety from the IEPOX or glycolic acid sulfate (GAS) OS, neither of which was detected in the  
570 supermicron aerosol (Froyd et al., 2009, 2019; Liao et al., 2015) (see Fig. S8). However,  $OS_f$  is  
571 much less than zero for ATom-2 ( $OS_f \sim -23\%$ ) and KORUS-AQ ( $OS_f \sim -26\%$ ). These  
572 unreasonable results may be due to the effect of OA on sulfate fragmentation in the AMS  
573 (discussed in Sect. 3.2). For this reason, strong caution is advised in applying  $OS_f$  estimation  
574 methods to ambient data, even in regime II. In addition, estimating OS with sulfate ions may be  
575 susceptible to errors due to inaccuracies in AS calibrations, noise present in the ambient data, or  
576 other factors.

577 We also show results from applying the Song et al. (2019) method in regime II (which is  
578 based on similar principles to the Chen method) in Fig. S9. Similarly to the Chen method, we see  
579 that most  $OS_f$  values are predicted to be less than zero. For the entire atmosphere, shown in Fig.  
580 S10, the distribution for  $OS_f$  looks similar to Fig. S9.

581 Regime III is characterized by high  $AN_f$  ( $> 0.3$ ) and lower acidity (calculated pH  $> 0$ ).  
582 This chemical regime primarily exists in polluted continental regions near large source regions  
583 such as megacities and agricultural regions, as high  $NO_x$  and  $NH_3$  emissions can lead to  
584 increased particulate AN and an increase in aerosol pH (Pye et al., 2019). In this regime, there  
585 are strong variations in the AMS sulfate fragments that are driven by  $AN_f$ .  $OS_f$  cannot be  
586 estimated with the AMS sulfate fragmentation methods proposed so far, unless they are further  
587 modified to account for the  $AN_f$  effect.  $\sim 31\%$  of KORUS-AQ data falls in this regime, but

588 almost none of the data from the rural / remote campaigns falls in this region, as AN typically  
589 evaporates as the air is diluted during advection away from polluted regions (DeCarlo et al.,  
590 2008).

591 Finally, regime IV in the top left quadrant has high AN ( $AN_f > 0.3$ ) and high acidity  
592 (calculated  $pH < 0$ ). This chemical regime is unlikely to be observed in the real atmosphere, and  
593 indeed there are very few points in that region for our campaigns. Sulfate is ubiquitous (Zhang et  
594 al., 2007b; Hodzic et al., 2020), and nitrate is not thermodynamically stable in the aerosol phase  
595 together with acidic sulfate for calculated  $pH < 0$  (Guo et. al., 2016). For all campaigns we  
596 observe  $\sim 0\%$  of points occupying this regime. Very unusual datapoints can be observed when  
597 ammonium nitrate-containing particles are externally mixed with acidic sulfate containing  
598 particles in an airmass.

599 Since the field studies analyzed here targeted large regions but did not sample many  
600 others, it is of interest to evaluate the fraction of the troposphere located in each one of the  
601 chemical regimes. The results of the GEOS-Chem v12 model are used for this purpose in Fig. 3B  
602 and shown as a global map in Fig. 4 and Fig. S11.  $\sim 67\%$  of the model troposphere exists in  
603 regime I (calculated  $pH < 0$ ). In addition,  $\sim 33\%$  of the global troposphere exists in regime II  
604 where it may be feasible to estimate  $OS_f$  from AMS fragments. Less than 1% of the modeled  
605 atmosphere exists in regime III (upper right quadrant) where ammonium nitrate strongly  
606 influences sulfate fragmentation, consistent with the relatively small very polluted geographical  
607 regions with very large  $AN_f$ . Finally, none of the data fell in regime IV, consistent with aerosols  
608 being assumed to be internally mixed in GEOS-Chem. At the surface during December, January,  
609 and February (DJF) (Fig. 4A), most of the remote oceans fall in regime I (calculated  $pH < 0$  and

610  $AN_f < 0.3$ ), while regime II (calculated  $pH > 0$  and  $AN_f < 0.3$ ) is dominant over continental  
611 regions. At the surface in June, July, and August (JJA) (Fig. 4C), most of the globe is in regime  
612 II. Very little of the data falls in regime III, except parts of Asia, regardless of season. A similar  
613 pattern is observed in the free troposphere (Fig. 4B and 4D) with some geographical differences.  
614 Regime III (calculated  $pH > 0$  and  $AN_f > 0.3$ ), which represents pollution hotspots, is observed in  
615 a large region in Asia during the Summer months, whereas the Winter months are dominated by  
616 regime I (low pH). The Summer months in the free troposphere are also mostly in regime II,  
617 especially over continental regions. Due to averaging of an entire year, as well as the limited  
618 spatial resolution of the GEOS-Chem model, locations and periods of high  $AN_f$  hotspots are not  
619 as prominent in these results, even when the data are divided by season.

## 620 **3.5 Potential pH estimation from AMS measurements**

### 621 **3.5.1 Estimation of pH from AMS sulfate fragments**

622 In Sect. 3.4, we introduced chemical regime I with low calculated pH and low  $AN_f$ . In  
623 this regime, which encompasses about half of the campaign data and  $\frac{2}{3}$  of the modeled global  
624 troposphere, PALMS data shows that the overwhelming majority of the sulfate is inorganic, with  
625  $OS_f$  contributing  $\sim 0.7\%$  to total sulfate by mass during ATom-1 and ATom-2 when calculated pH  
626  $< 0$  (see Fig. S8, in regime I). This removes sulfate fragmentation changes caused by AN and  
627 sulfate type (OS vs. AS), indicating that sulfate fragmentation is almost exclusively controlled by  
628 the acidity of the aerosol. Fig. 1C shows that  $fH_2SO_4^+$  and  $fHSO_3^+$ , i.e. the amount of sulfate  
629 fragments retaining one or two hydrogens ( $H_2SO_4^+$  and  $HSO_3^+$ ) relative to the total sulfate  
630 fragments ( $H_2SO_4^+$ ,  $HSO_3^+$ ,  $SO_3^+$ ,  $SO_2^+$ , and  $SO^+$ ) increases as calculated pH decreases.

631 In Fig. 5 we show the relationship between  $H_ySO_x^+/SO_x^+$  and aerosol pH. As the  
632 relationship is noisy for individual data points, we show the results for 5% quantiles of the data.  
633  $H_ySO_x^+/SO_x^+$  appears to show a proportional relationship with decreasing calculated pH for the  
634 ATom campaigns, for which much of the data is in regime I. The KORUS-AQ data, of which  
635 very little falls in the regime I, does not show a relationship between these variables, as expected.  
636 A fitted equation to the ATom relationship may allow the real-time estimation of pH for different  
637 air masses for campaigns in regime I as:

$$pH = -1.3 (\pm 0.06) + 6.0(\pm 1.2) \times e^{-1.3(\pm 0.18) \times \frac{H_ySO_x^+}{SO_x^+}} \quad \text{Eq. 13}$$

638 As shown in the histogram in Fig. 5B, this relationship is applicable to a substantial fraction of  
639 ambient observations. This estimation equation likely needs to be calibrated for each instrument  
640 (e.g. by sampling sulfate particles with different acidities), since the sulfate fragmentation does  
641 vary with instrument (Chen et al., 2019) and potentially also in time for a given instrument.

642 Although an estimation equation that apparently works for only one unit of pH may seem  
643 of limited value, two caveats apply: first, it is of high value to know that the estimated  $pH < 0$  for  
644 a certain air mass (as opposed to e.g. estimated  $pH = 2$  or  $3$  that are frequently encountered).  
645 Second, the range of estimated pH below 0 is limited here due to not considering the activity  
646 coefficient. If that coefficient was included, the predicted estimated pH range in this regime  
647 would be  $\sim -4$  to 0.

### 648 3.5.2 Estimation of pH from Ammonium Balance

649 Ammonium balance ( $NH_{4\_bal}$ ) (Eq. (7)) is often used as a qualitative indicator of acidity.  
650 (Zhang et al., 2007a) showed that calculated pH under constant temperature and RH was well

651 correlated with ammonium balance, but much more scatter was observed when the instantaneous  
652 T and RH were used. Several studies have argued that ammonium balance cannot be used to  
653 estimate ambient pH (e.g., Guo et al., 2015, 2016; Hennigan et al., 2015; Weber et al., 2016);  
654 however, those studies were all performed at continental ground sites that were in the less-acidic  
655 chemical regimes (II and III), and where daily temperature and humidity changes were strong.  
656 As shown in Fig. 6,  $NH_{4\_bal}$  and calculated pH for the aircraft studies show a strong and  
657 consistent relationship in regime I (calculated pH < 0), providing another potential method for  
658 estimating pH (all one needs to use this method is the ammonium balance, and if it is < 0.65, the  
659 method should be applicable). As ammonium balance increases, so does calculated pH across the  
660 six campaigns studied. These data are generally outside of the continental boundary layer, where  
661 temperature and RH change less in a diurnal cycle, reducing the impact of those changes on pH.  
662 For data in regimes II-III (calculated pH > 0) some proportionality of pH and  $NH_{4\_bal}$  is still  
663 observed on average, but with more dispersion across campaigns. Given the similarity of the  
664 results for regime I, the fitting equation of calculated pH vs. ammonium balance may be used to  
665 provide a near real-time estimate of pH (for  $NH_{4\_bal} < 0.65$ ).

$$pH = -1.1(\pm 0.031) + 1.7(\pm 0.089) * NH_{4\_bal} \quad \text{Eq. 14}$$

666 As shown in the histogram in Fig 6B-6D, this relationship is also applicable to a  
667 substantial fraction of ambient regions. This estimation equation should be tested with other  
668 studies. An advantage of this relationship (vs. the one based on  $H_ySO_x^+/SO_x^+$ ) is that it is likely to  
669 be less instrument-dependent, as long as careful calibrations of  $RIE_{NH_4}$  and  $RIE_{SO_4}$  have been  
670 performed. Conditions where non-volatile cations (e.g.  $Na^+$ ,  $K^+$ ,  $Ca^{2+}$ ) are important for  
671 submicron particles could lead to deviations from this relationship (Guo et al., 2020). However,



672 such conditions are infrequent in remote air (Nault et al., 2020) and can be diagnosed by  
673 concurrent supermicron or filter measurements.

### 674 **3.5.3 Application of pH estimation methods to ambient data**

675 As discussed above, ammonium balance and  $\text{H}_y\text{SO}_x^+/\text{SO}_x^+$  are two measurements that  
676 may be used to estimate aerosol acidity in parts of the atmosphere. In Fig. 7 these two methods  
677 are applied to one flight during ATom-1 and an  $\text{SO}_2$  plume sampled during WINTER. In Fig. 7A,  
678 both  $\text{H}_y\text{SO}_x^+/\text{SO}_x^+$  and  $\text{NH}_{4\_bal}$  follow the trend for E-AIM calculated pH during most periods  
679 when calculated  $\text{pH} < 0$ , even at one minute time resolution.

680 As expected from Fig. 6,  $\text{NH}_{4\_bal}$  is a less noisy, more robust metric for estimating pH at  
681 one minute time resolution. Unlike  $\text{H}_y\text{SO}_x^+/\text{SO}_x^+$ ,  $\text{NH}_{4\_bal}$  appears to be able to capture basic  
682 calculated pH trends at the full range of calculated pH values observed during this flight in  
683 ATom-1.  $\text{NH}_{4\_bal}$  also matches the E-AIM calculated pH well for the WINTER power plant  
684 plume. For RF01 in ATom-1 (WINTER),  $\text{NH}_{4\_bal}$  estimated pH has an  $R^2 \sim 0.6$  (0.9) for  $\text{pH} < 0$   
685 (Fig. 7C-D). This shows that in the remote atmosphere (like in ATom) or in an  $\text{SO}_2$  plume,  $\text{NH}_{4\_bal}$   
686 has the potential to allow fast estimation of pH, even under relatively low sulfate concentrations,  
687 albeit not perfectly. More scatter is observed for the estimate based on  $\text{H}_y\text{SO}_x^+/\text{SO}_x^+$ , indicating  
688 that longer averages are needed for this method. The error is typically within  $\pm 0.5$  estimated  
689 pH units, which is thought to be the accuracy of thermodynamic pH estimation models.

### 690 **3.6 Possibility of Estimating Collection Efficiency (CE) from Sulfate Fragmentation**

691 From the previous discussion it is clear that sulfate fragmentation changes due to some of  
692 the same factors (acidity,  $AN_f$ ) that influence ambient AMS CE. It is of interest to explore  
693 whether a quantitative estimate of ambient particle CE could be derived from the measured  
694 sulfate fragments, at least under some conditions, as it could provide a complementary  
695 characterization to the CE estimates from the Middlebrook et al. (2012) parameterization. In Fig.  
696 8 we show the CE estimated from Middlebrook et al. (2012) vs.  $H_ySO_x^+/SO_x^+$  for ATom and  
697 KORUS-AQ. CE does show some relationship with  $H_ySO_x^+/SO_x^+$ , with most sensitivity around  
698  $CE \sim 0.8-0.9$ . A substantial level of noise is observed on the high-time resolution data, and the  
699 trend varies between the two campaigns (where variations in CE are controlled by two different  
700 effects, acidity vs  $AN_f$ ). Further research would be necessary to evaluate whether this method  
701 could be used to estimate CE.

## 702 **Conclusions**

703 The presence of organosulfates in particles is a topic of much recent interest, but there is  
704 a lack of online methods to quantify them. Two methods have been proposed to use widely  
705 available AMS data to quantify  $OS_f$  (Chen et al., 2019; Song et al., 2019). These methods have  
706 only been applied to ground continental datasets, to our knowledge. We show using both  
707 laboratory and field data that both high acidity (regime I) and high  $AN_f$  (regime III) result in  
708 major changes in sulfate fragmentation, which often lead to nonsensical results for the  $OS_f$   
709 methods. Regime I accounts for  $\sim 2/3$  of the global troposphere, while regime III can be  
710 important in polluted regions (e.g. Seoul region), and thus it is critical to avoid applying the  
711 proposed  $OS_f$  estimation methods in these regimes. In regime II, with lower acidity and lower

712 nitrate (calculated  $\text{pH} > 0$ ,  $\text{AN}_f < 0.3$ )  $\text{OS}_f$  estimation methods may be applicable, if no other  
713 effects (e.g. significant non-volatile cations or variations in OA effects) confound the sulfate  
714 fragmentation. For the ambient data analyzed here, even in regime II the  $\text{OS}_f$  estimation  
715 produced nonsensical results. Extreme caution is recommended to anyone who chooses to apply  
716 the  $\text{OS}_f$  estimation methods. For reasons not fully understood, fragmentation of the sulfate ions  
717 in the lab vs. ambient data differ at times.

718         We investigated two different methods to estimate pH in real-time in regime I (calculated  
719  $\text{pH} < 0$  and  $\text{AN}_f < 0.3$ ), based on the AMS  $\text{H}_y\text{SO}_x^+/\text{SO}_x^+$  fragment ratio and the ammonium  
720 balance, respectively, without the need to run a thermodynamic model, and without the need for  
721 gas-phase  $\text{NH}_3$  or  $\text{HNO}_3$  measurements. Low  $\text{OS}_f$  and non-volatile cations need to be assumed or  
722 confirmed from AMS and other measurements. The ammonium balance method shows better  
723 performance. These *in-situ* and direct pH estimation methods should be applicable in the remote  
724 atmosphere (oceanic regions, and often the continental free troposphere when not recently  
725 impacted by surface sources). Both the  $\text{OS}_f$  and pH estimations require careful instrument  
726 calibration for a given campaign, and the methods based on sulfate fragments are expected to be  
727 instrument-dependent, including for the same instrument in time when filaments or the vaporizer  
728 are replaced, or when the instrument is re-tuned. Both methods should be further evaluated with  
729 data from other studies.

730         We propose a conceptual model to explain the observed sulfate fragmentation changes  
731 with changing particle chemical composition. As particles become more acidic or higher in AN,  
732 a higher fraction of  $\text{H}_2\text{SO}_4(\text{g})$  can reach the ionization region, leading to changes in the observed  
733 ion population. Since AMS CE is thought to be controlled by the same effects, we explore

734 whether it can be estimated from the observed sulfate fragmentation, and find that while changes  
735 in  $\text{H}_y\text{SO}_x^+/\text{SO}_x^+$  do correlate to changes in CE, the relationship is not the same across different  
736 campaigns. Further investigation of this relationship, especially when direct CE measurements  
737 are available via internal AMS light scattering, would be of interest.

738         We have not explored the application of these methods to ACSM data. ACSM data are  
739 unit-mass resolution, and the interferences between species at a given unit mass are estimated  
740 using a fragmentation table approach (Allan et al., 2004). This approach introduces more  
741 uncertainties, as exemplified by Hu et al. (2015) for similar fragment-based methods.

## 742 **Acknowledgements**

743 This work was supported by NASA grants NNX15AH33A & 80NSSC19K0124, and a CIRES  
744 IRP project. We thank the members of the Jimenez group, the AMS users community, Weiwei  
745 Hu, Amber Ortega, and Patrick Hayes for help with data acquisition during SEAC<sup>4</sup>RS and DC-3;  
746 Jason St. Clair, Alex Teng, Michelle Kim, John Crouse, and Paul Wennberg for providing  
747 CIT-CIMS  $\text{HNO}_3$  data; Joel Thornton, Felipe Lopez-Hilfiker, and Ben Lee for providing  
748 UW-CIMS  $\text{HNO}_3$  data during WINTER; Karl Froyd, Gregory P. Schill, and Daniel Murphy for  
749 providing PALMS organosulfate data for ATOm campaigns; and Glenn Diskin for providing  
750 DLH  $\text{H}_2\text{O}$  data.

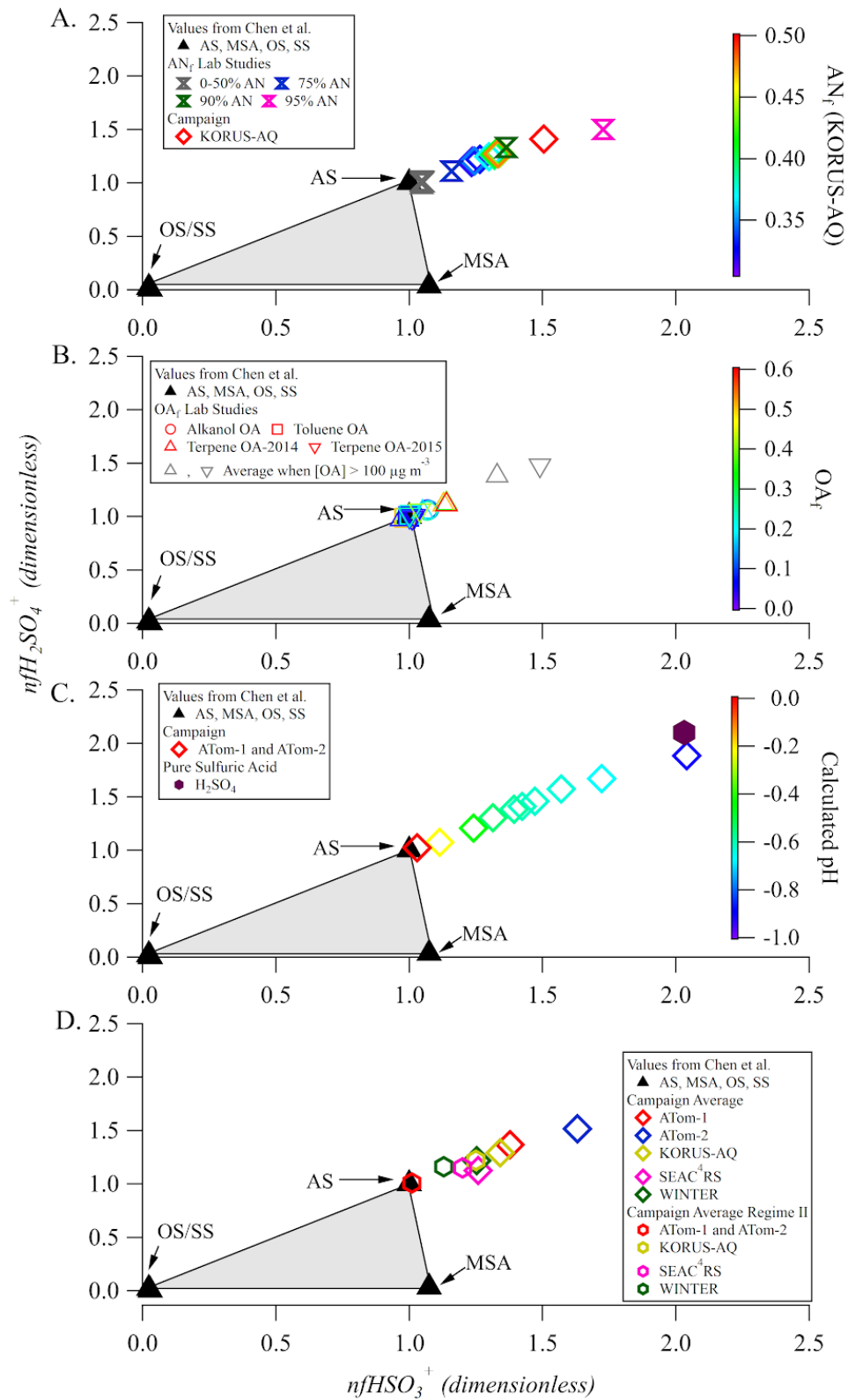
## 751 **Data Availability**

752 DC3 data available at [DOI: 10.5067/Aircraft/DC3/DC8/Aerosol-TraceGas](https://doi.org/10.5067/Aircraft/DC3/DC8/Aerosol-TraceGas), last accessed on 9  
753 September, 2018. SEAC<sup>4</sup>RS data available at  
754 <http://doi.org/10.5067/Aircraft/SEAC4RS/Aerosol-TraceGas-Cloud>, last accessed on 27 April,  
755 2020. WINTER data available at [https://data.eol.ucar.edu/master\\_lists/generated/winter/](https://data.eol.ucar.edu/master_lists/generated/winter/), last  
756 accessed 27 April 2020. KORUS-AQ data available at [DOI:](https://doi.org/10.5067/Suborbital/KORUSAQ/DATA01)  
757 [10.5067/Suborbital/KORUSAQ/DATA01](https://doi.org/10.5067/Suborbital/KORUSAQ/DATA01), last accessed 14 June, 2018. ATOm-1 and ATOm-2  
758 data available at <https://doi.org/10.3334/ORNLDAAC/158>, last accessed 27 April 2020.

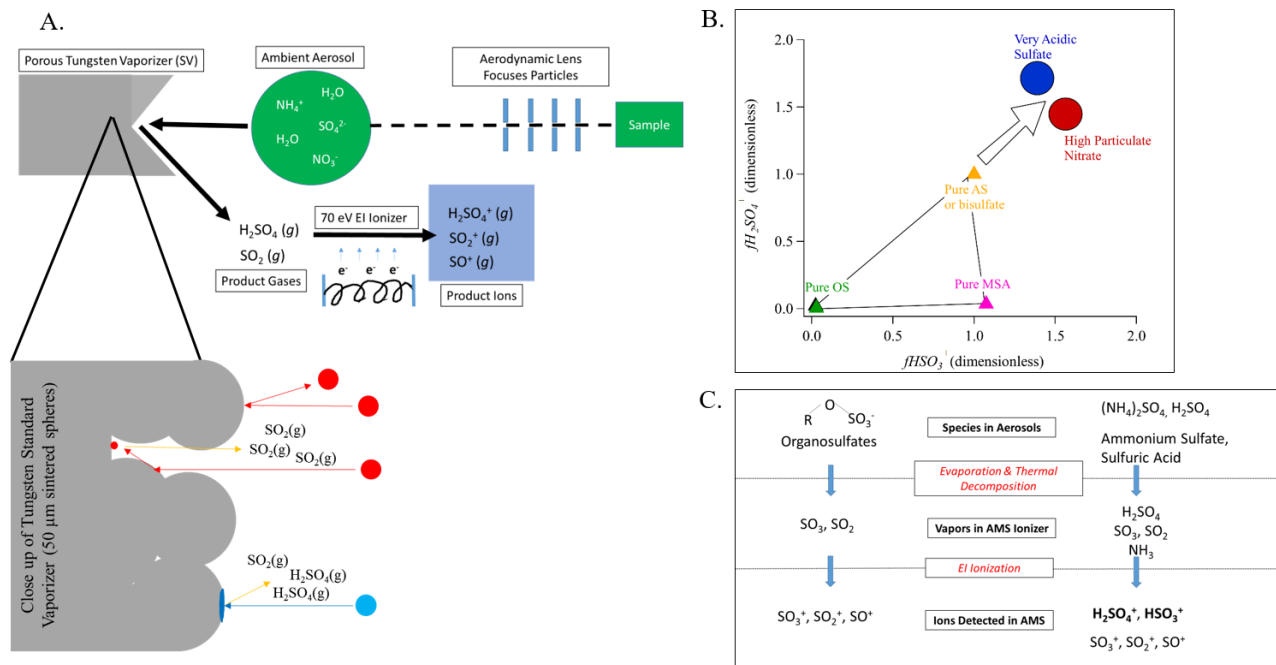
759 **Tables and Figures**

760 *Table 1. Summary of the campaigns used in this study. See SI Fig. S1 for flight paths. Reference*  
 761 *label refers to the type of data used for each campaign throughout this paper, depending on the*  
 762 *quality and completeness of the data, for the purposes of a specific analysis. A : ammonium*  
 763 *balance, f: SO<sub>4</sub> campaign-averaged fragments, F: SO<sub>4</sub> campaign-average and time-resolved*  
 764 *fragments , and C: pure AS calibration data reliable and used.*

| Campaign  | Location                                      | Season/Year                       | References   | Reference Label |
|---|---|-----------------------------------|--|-----------------|
| DC3: Deep Convective Clouds and Chemistry   | Mid-Latitude Continental United States        | Spring/Summer 2012                | Barth et al., (2015)   | A               |
| SEAC <sup>4</sup> RS: Studies of Emissions and Atmospheric Composition, Clouds and Climate Coupling by Regional Surveys | Continental United States                     | Summer 2013                       | Wagner et al., (2015); Toon et al., (2016)                   | A, f, C         |
| WINTER: Wintertime Investigation of Transport, Emissions, and Reactivity  | Eastern United States, continental and marine | Winter 2015                       | Jaeglé et al., (2018); Schroder et al., (2018)               | A, f, C         |
| KORUS-AQ: Korean United States Air Quality  | South Korean Peninsula and Yellow Sea         | Spring 2016                       | Nault et al., (2018)   | A, F, C         |
| ATom-1: Atmospheric Tomography Mission 1  | Remote Pacific and Atlantic Basins            | Boreal Summer/Austral Winter 2016 | Brock (2019); Hodshire et al., (2019); Hodzic et al., (2020) | A, F, C         |
| ATom-2: Atmospheric Tomography Mission 2  | Remote Pacific and Atlantic Basins            | Austral Summer/Boreal Winter 2017 | Hodzic et al., (2020)  | A, F, C         |

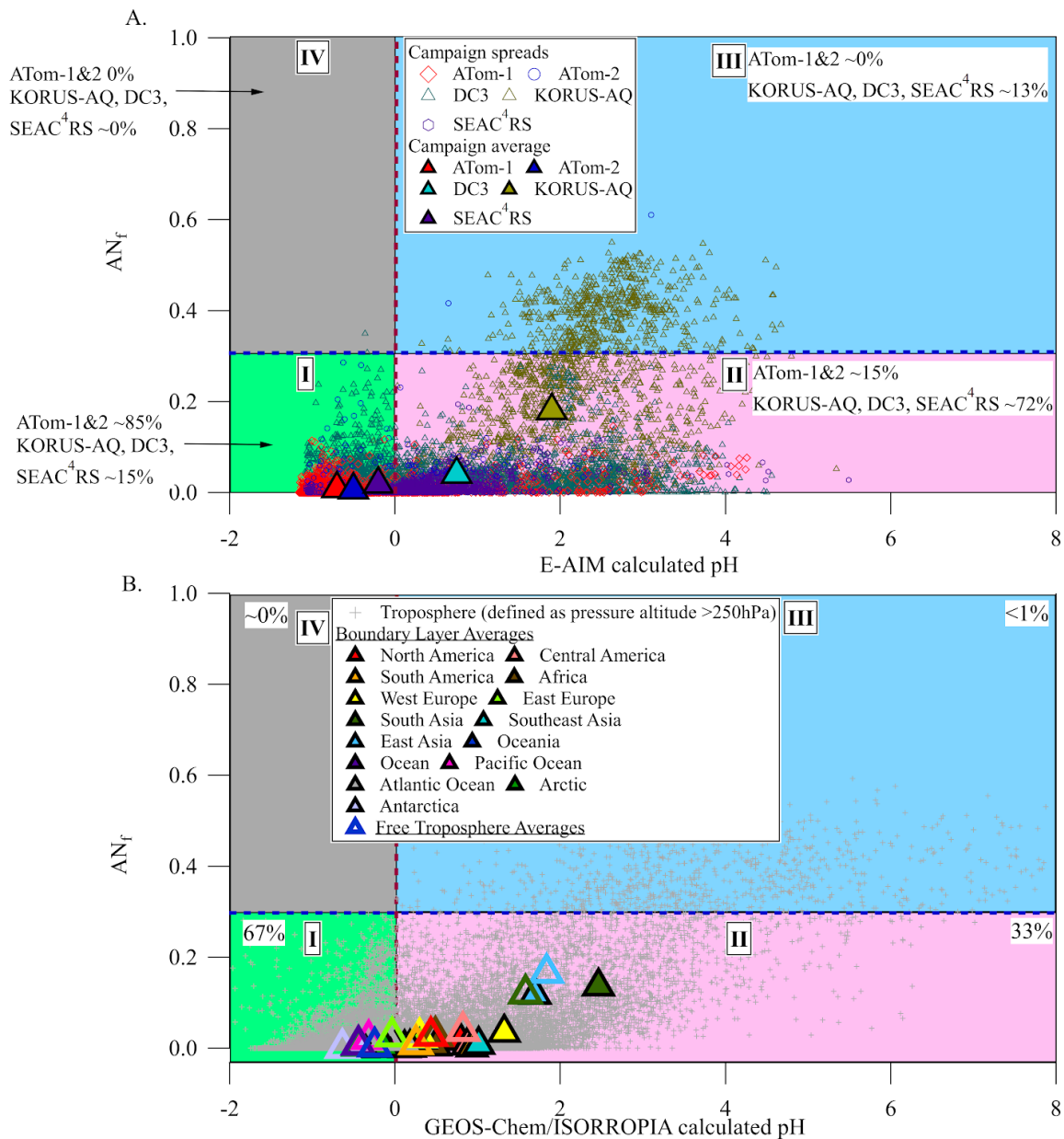


765 Fig. 1. Laboratory and field data for sulfate fragmentation shown in the triangle diagram  
766 proposed by Chen et al. (2019). (A) Data split into 10 quantiles of  $AN_f$  value for the full  
767 KORUS-AQ campaign, as well as for different laboratory internal mixtures of AS and AN. (B)  
768 Data from two chamber experiments, split into 5 quantiles of  $OA_f$ . Data with very high OA  
769 ( $>100 \mu\text{g m}^{-3}$ ) are shown as grey triangles. The average of  $OA_f$  for the very high OA data in 2014  
770 and 2015 is 0.8. Two separate datasets of monoterpene SOA chamber experiments are labelled as  
771 “2014” and “2015”. (C) Data split into 10 quantiles by calculated pH for ATom-1 and 2, colored  
772 by calculated pH from E-AIM. (D) Averages for 5 aircraft campaigns for the full campaign and a  
773 subset of each campaign where  $\text{pH} < 0$  and  $AN_f < 0.3$ .

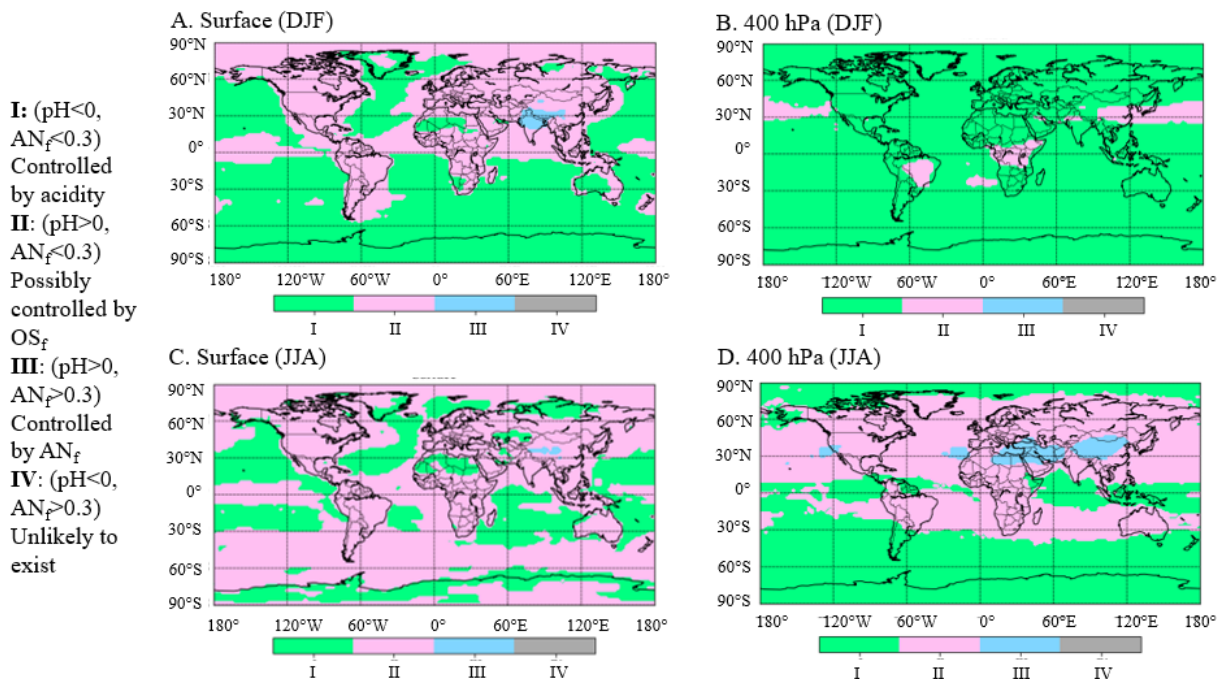


774 Fig. 2. (A) Simplified schematic of the AMS detection process, including a close up of the  
 775 tungsten standard vaporizer surface and the different species produced by AS and OS. (B)  
 776 Conceptual model of the position of particles of different compositions in the Chen et al. (2019)  
 777 triangle plot. As particles become more acidic or higher in particulate nitrate, the ratio of the  
 778 AMS hydrogenated to total sulfate fragments increases. When sulfate is present as AS (or  
 779 mixtures of AS and ammonium bisulfate), the sulfate fragmentation is mainly impacted by OS  
 780 vs. AS vs. MSA relative concentrations inside the Chen triangle. (C) Schematic of the  
 781 transformations during the AMS detection process for OS and AS.

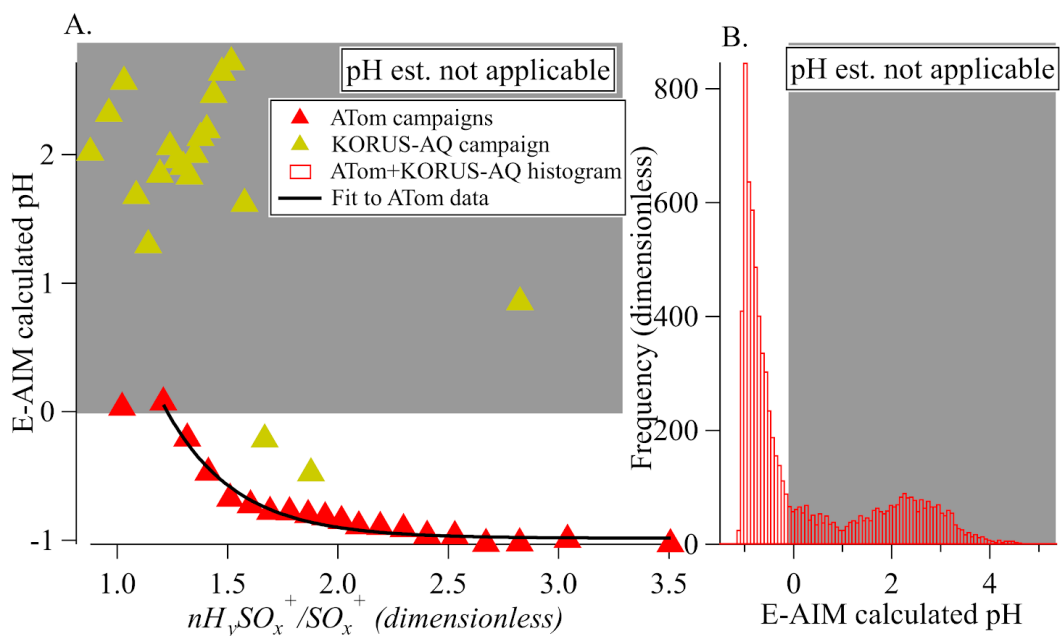




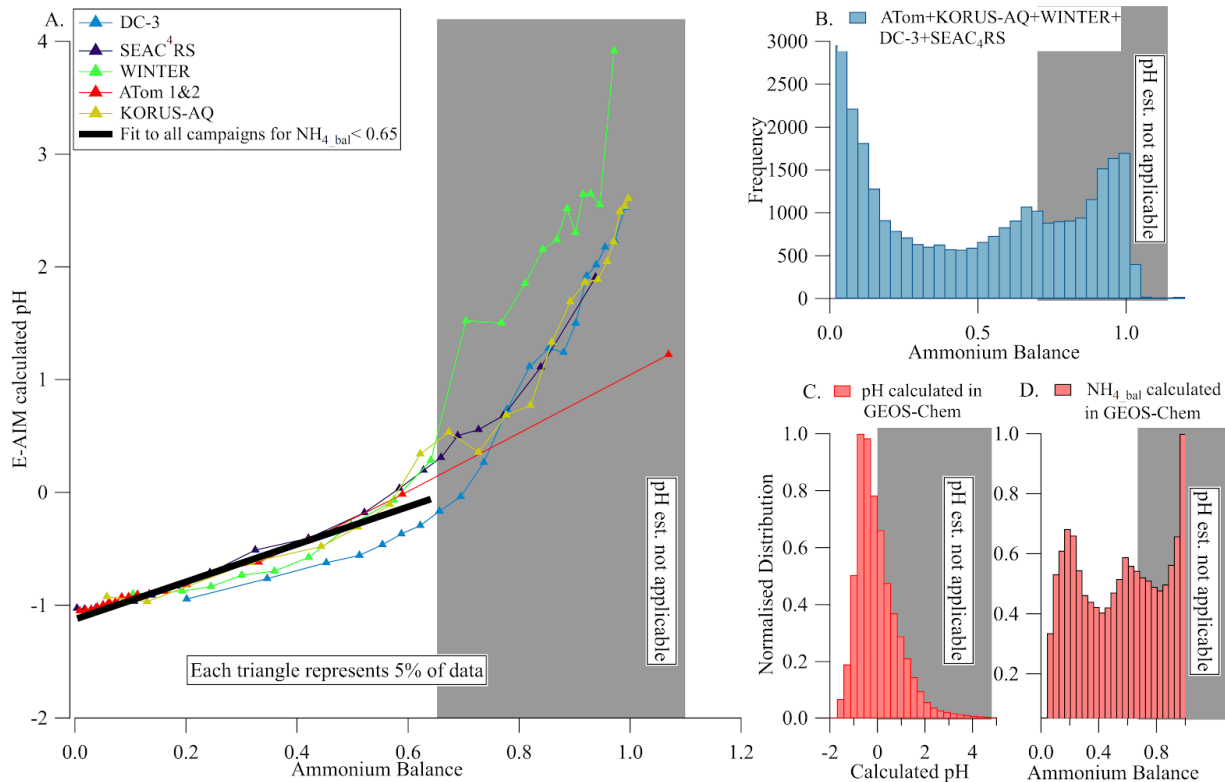
782 Fig. 3. (A) location of the aircraft campaign 1-minute data points on the chemical regimes  
 783 defined in this paper ( $AN_p$ , from AMS measurements) vs. E-AIM pH. SEAC<sup>4</sup>RS, WINTER, and  
 784 KORUS-AQ are averaged to one value, for brevity, but defined individually in Sect. 3.4. (B)  
 785 Location of global GEOS-Chem v12 results in the chemical-regimes diagram. Yearlong averages  
 786 shown as large triangles.



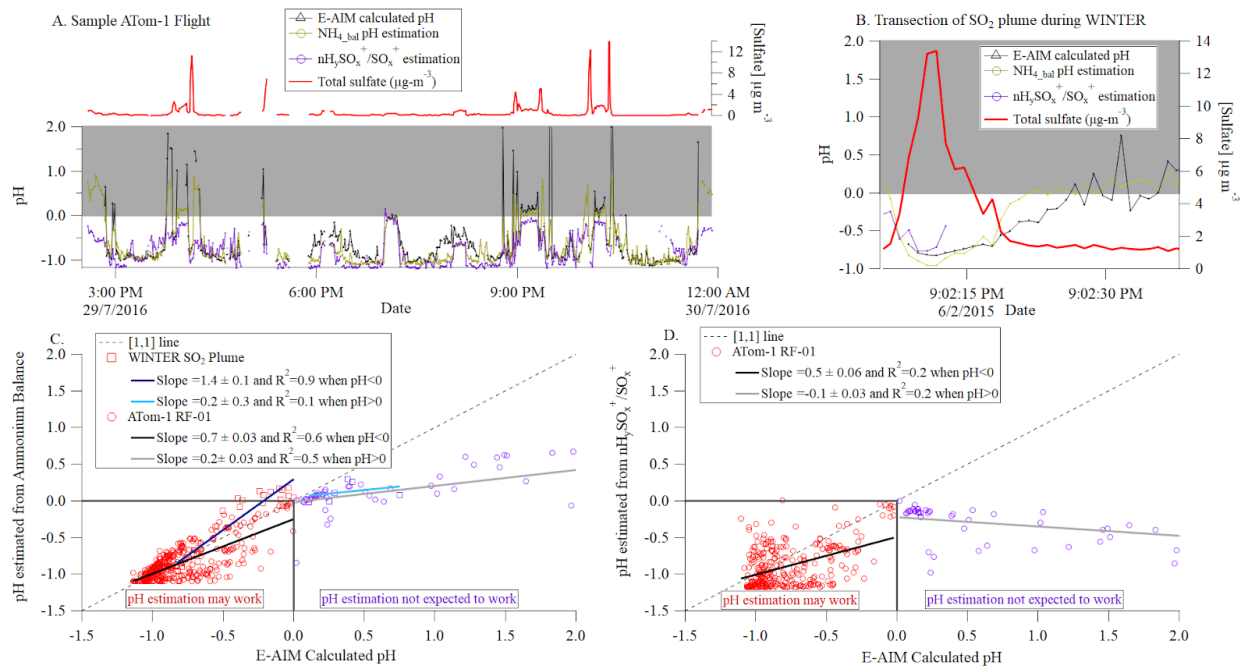
787 Fig. 4. Areas characterized by different chemical regimes according to results from  
 788 GEOS-Chem v12. (A) Surface for December, January, and February (DJF), (B) 400 hPa for DJF,  
 789 (C) Surface for June, July, and August (JJA), (D) 400 hPa for JJA. Roman numerals correspond  
 790 to regimes in Fig. 3.



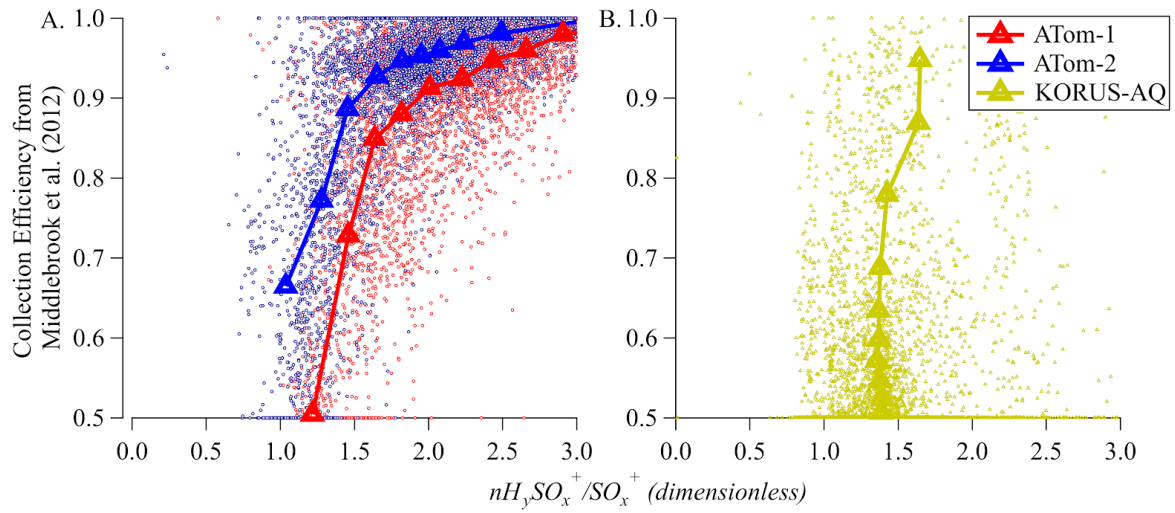
791 Fig. 5. (A) Calculated pH vs. sulfate fragmentation indicator ( $H_ySO_x^+/SO_x^+$ ) for the ATom and  
 792 KORUS-AQ campaigns, and binned by  $nH_ySO_x^+/SO_x^+$ . The black line is an exponential fit to  
 793 ATom data (see text) when calculated  $pH < 0$ . (B) histogram of the calculated pH for the 1-minute  
 794 datapoints from the ATom-1,2 and KORUS-AQ datasets. In both panels, the white (gray) area  
 795 shows the regime where calculated pH can (and cannot) be estimated from the sulfate  
 796 fragmentation.



797 Fig. 6. (A) Calculated pH vs. ammonium balance for multiple campaigns. Quantiles of the data  
 798 are used to reduce the impact of noise. The black line is an orthogonal distance regression (ODR)  
 799 fit to the campaign data for values with  $\text{NH}_4_{\text{Bal}} < 0.65$ . B) Histogram of measured ammonium  
 800 balance for the 6 campaigns. (C) and (D), calculated pH and ammonium balance from  
 801 GEOS-Chem (pH calculated with ISORROPIA). In all panels the white (grey) areas encompass  
 802 the data points for which calculated pH can (and cannot) be estimated from the measured  
 803 ammonium balance.



804 Fig. 7. (A) Time series of sulfate, pH calculated from E-AIM and estimated from  $\text{H}_y\text{SO}_x^+/\text{SO}_x^+$ ,  
 805 and  $\text{NH}_4_{\text{Bal}}$  for one flight during ATom-1 (at 1 min. resolution, filtered to remove points where  
 806 sulfate was less than 3 times its detection limit). (B) Time series of sulfate and pH for a large  
 807 power plant plume sampled during WINTER, only a few data points are shown for pH estimated  
 808 from  $\text{nH}_y\text{SO}_x^+/\text{SO}_x^+$  because sulfate in the AMS evaporated slowly during the second half of the  
 809 plume transect, leading to altered sulfate fragmentation, and this effect cannot be corrected for,  
 810 due to infrequent backgrounds in aircraft fast acquisition mode. (C) Scatter Plot of estimated pH  
 811 predicted from  $\text{NH}_4_{\text{Bal}}$  vs. E-AIM calculated pH for the data above. (D) Scatterplot of estimated  
 812 pH predicted from  $\text{nH}_y\text{SO}_x^+/\text{SO}_x^+$  vs. E-AIM calculated pH for the ATom flight.



813 Fig. 8. (A) Collection efficiency parameterization vs.  $nH_ySO_x^+/SO_x^+$  for two ATom campaigns,  
 814 and (B) the KORUS-AQ campaign.

## 815 References

- 816 Ackendorf, J. M., Ippolito, M. G. and Galloway, M. M.: pH Dependence of the  
817 Imidazole-2-carboxaldehyde Hydration Equilibrium: Implications for Atmospheric Light  
818 Absorbance, *Environ. Sci. Technol. Lett.*, 4(12), 551–555, doi:10.1021/acs.estlett.7b00486,  
819 2017.
- 820 Alfarra, M. R., Coe, H., Allan, J. D., Bower, K. N., Boudries, H., Canagaratna, M. R., Jimenez, J.  
821 L., Jayne, J. T., Garforth, A. A., Li, S.-M. and Worsnop, D. R.: Characterization of urban and  
822 rural organic particulate in the Lower Fraser Valley using two Aerodyne Aerosol Mass  
823 Spectrometers, *Atmos. Environ.*, 38(34), 5745–5758, doi:10.1016/j.atmosenv.2004.01.054, 2004.
- 824 Allan, J. D., Delia, A. E., Coe, H., Bower, K. N., Alfarra, M. R., Jimenez, J. L., Middlebrook, A.  
825 M., Drewnick, F., Onasch, T. B., Canagaratna, M. R., Jayne, J. T. and Worsnop, D. R.: A  
826 generalised method for the extraction of chemically resolved mass spectra from Aerodyne  
827 aerosol mass spectrometer data, *J. Aerosol Sci.*, 35(7), 909–922,  
828 doi:10.1016/j.jaerosci.2004.02.007, 2004.
- 829 Anon: Atmospheric chemistry and physics: from air pollution to climate change, *Choice*  
830 *Reviews Online*, 44(08), 44–4512–44–4512, doi:10.5860/CHOICE.44-4512, 2007.
- 831 Bahreini, R., Dunlea, E. J., Matthew, B. M., Simons, C., Docherty, K. S., DeCarlo, P. F., Jimenez,  
832 J. L., Brock, C. A. and Middlebrook, A. M.: Design and Operation of a Pressure-Controlled Inlet  
833 for Airborne Sampling with an Aerodynamic Aerosol Lens, *Aerosol Sci. Technol.*, 42(6),  
834 465–471, doi:10.1080/02786820802178514, 2008.
- 835 Bahreini, R., Ervens, B., Middlebrook, A. M., Warneke, C., de Gouw, J. A., DeCarlo, P. F.,  
836 Jimenez, J. L., Brock, C. A., Neuman, J. A., Ryerson, T. B., Stark, H., Atlas, E., Brioude, J.,  
837 Fried, A., Holloway, J. S., Peischl, J., Richter, D., Walega, J., Weibring, P., Wollny, A. G. and  
838 Fehsenfeld, F. C.: Organic aerosol formation in urban and industrial plumes near Houston and  
839 Dallas, Texas, *J. Geophys. Res.*, 114, 1185, doi:10.1029/2008JD011493, 2009.
- 840 Barth, M. C., Cantrell, C. A., Brune, W. H., Rutledge, S. A., Crawford, J. H., Huntrieser, H.,  
841 Carey, L. D., MacGorman, D., Weisman, M., Pickering, K. E., Bruning, E., Anderson, B., Apel,  
842 E., Biggerstaff, M., Campos, T., Campuzano-Jost, P., Cohen, R., Crouse, J., Day, D. A., Diskin,  
843 G., Flocke, F., Fried, A., Garland, C., Heikes, B., Honomichl, S., Hornbrook, R., Huey, L. G.,  
844 Jimenez, J. L., Lang, T., Lichtenstern, M., Mikoviny, T., Nault, B., O’Sullivan, D., Pan, L. L.,  
845 Peischl, J., Pollack, I., Richter, D., Riemer, D., Ryerson, T., Schlager, H., St. Clair, J., Walega, J.,  
846 Weibring, P., Weinheimer, A., Wennberg, P., Wisthaler, A., Wooldridge, P. J. and Ziegler, C.: The  
847 Deep Convective Clouds and Chemistry (DC3) Field Campaign, *Bull. Am. Meteorol. Soc.*,  
848 96(8), 1281–1309, doi:10.1175/BAMS-D-13-00290.1, 2015.
- 849 Bertram, T. H. and Thornton, J. A.: Toward a general parameterization of N<sub>2</sub>O<sub>5</sub> reactivity on  
850 aqueous particles: the competing effects of particle liquid water, nitrate and chloride, *Atmos.*

851 Chem. Phys., 9(21), 8351–8363, 2009.

852 Bey, I., Jacob, D. J., Yantosca, R. M., Logan, J. A., Field, B. D., Fiore, A. M., Li, Q., Liu, H. Y.,  
853 Mickley, L. J. and Schultz, M. G.: Global modeling of tropospheric chemistry with assimilated  
854 meteorology: Model description and evaluation, *J. Geophys. Res.*, 106(D19), 23073–23095,  
855 doi:10.1029/2001JD000807, 2001.

856 Brock, C.: Aerosol size distributions during the Atmospheric Tomography (ATom) mission:  
857 methods, uncertainties, and data products, *Aerosols/In Situ Measurement/Instruments and*  
858 *Platforms/amt-2019-44*, doi:10.5194/amt-2019-44-ac1, 2019.

859 Brüggemann, M., Riva, M., Perrier, S., Poulain, L., George, C. and Herrmann, H.:  
860 Overestimation of Monoterpene Organosulfate Abundance in Aerosol Particles by Sampling in  
861 the Presence of SO<sub>2</sub>, *Environ. Sci. Technol. Lett.*, doi:10.1021/acs.estlett.0c00814, 2020.

862 Canagaratna, M. R., Jayne, J. T., Jimenez, J. L., Allan, J. D., Alfarra, M. R., Zhang, Q., Onasch,  
863 T. B., Drewnick, F., Coe, H., Middlebrook, A., Delia, A., Williams, L. R., Trimborn, A. M.,  
864 Northway, M. J., DeCarlo, P. F., Kolb, C. E., Davidovits, P. and Worsnop, D. R.: Chemical and  
865 microphysical characterization of ambient aerosols with the aerodyne aerosol mass spectrometer,  
866 *Mass Spectrom. Rev.*, 26(2), 185–222, doi:10.1002/mas.20115, 2007.

867 Carlton, A. G., de Gouw, J., Jimenez, J. L., Ambrose, J. L., Attwood, A. R., Brown, S., Baker, K.  
868 R., Brock, C., Cohen, R. C., Edgerton, S., Farkas, C. M., Farmer, D., Goldstein, A. H., Gratz, L.,  
869 Guenther, A., Hunt, S., Jaeglé, L., Jaffe, D. A., Mak, J., McClure, C., Nenes, A., Nguyen, T. K.,  
870 Pierce, J. R., de Sa, S., Selin, N. E., Shah, V., Shaw, S., Shepson, P. B., Song, S., Stutz, J.,  
871 Surratt, J. D., Turpin, B. J., Warneke, C., Washenfelder, R. A., Wennberg, P. O. and Zhou, X.:  
872 Synthesis of the Southeast Atmosphere Studies: Investigating Fundamental Atmospheric  
873 Chemistry Questions, *Bull. Am. Meteorol. Soc.*, 99(3), 547–567,  
874 doi:10.1175/BAMS-D-16-0048.1, 2018.

875 Chen, Y., Xu, L., Humphry, T., Hettiyadura, A. P. S., Ovadnevaite, J., Huang, S., Poulain, L.,  
876 Schroder, J. C., Campuzano-Jost, P., Jimenez, J. L., Herrmann, H., O’Dowd, C., Stone, E. A. and  
877 Ng, N. L.: Response of the Aerodyne Aerosol Mass Spectrometer to Inorganic Sulfates and  
878 Organosulfur Compounds: Applications in Field and Laboratory Measurements, *Environ. Sci.*  
879 *Technol.*, 53(9), 5176–5186, doi:10.1021/acs.est.9b00884, 2019.

880 Clegg, S. L., Brimblecombe, P. and Wexler, A. S.: Thermodynamic Model of the System H +  
881 -NH<sub>4</sub> + -SO<sub>4</sub><sup>2-</sup> -NO<sub>3</sub> -H<sub>2</sub>O at Tropospheric Temperatures, , 5639(3), 2137–2154, 1998a.

882 Clegg, S. L., Brimblecombe, P. and Wexler, A. S.: Thermodynamic Model of the System H  
883 -NH<sub>4</sub> -SO<sub>4</sub><sup>2-</sup>-NO<sub>3</sub>-H<sub>2</sub>O at Tropospheric Temperatures, *The Journal of Physical Chemistry*  
884 *A*, 102(12), 2137–2154, doi:10.1021/jp973042r, 1998b.

885 Clegg, S. L., Seinfeld, J. H. and Edney, E. O.: Thermodynamic modelling of aqueous aerosols  
886 containing electrolytes and dissolved organic compounds. II. An extended  
887 Zdanovskii–Stokes–Robinson approach, *J. Aerosol Sci.*, 34(6), 667–690,



888 doi:10.1016/S0021-8502(03)00019-3, 2003.

889 Craig, R. L., Peterson, P. K., Nandy, L., Lei, Z., Hossain, M. A., Camarena, S., Dodson, R. A.,  
890 Cook, R. D., Dutcher, C. S. and Ault, A. P.: Direct Determination of Aerosol pH: Size-Resolved  
891 Measurements of Submicrometer and Supermicrometer Aqueous Particles, *Anal. Chem.*, 90(19),  
892 11232–11239, doi:10.1021/acs.analchem.8b00586, 2018.

893 Crounse, J. D., McKinney, K. A., Kwan, A. J. and Wennberg, P. O.: Measurement of gas-phase  
894 hydroperoxides by chemical ionization mass spectrometry, *Anal. Chem.*, 78(19), 6726–6732,  
895 doi:10.1021/ac0604235, 2006.

896 Cubison, M. J., Ortega, A. M., Hayes, P. L., Farmer, D. K., Day, D., Lechner, M. J., Brune, W.  
897 H., Apel, E., Diskin, G. S., Fisher, J. A. and Others: Effects of aging on organic aerosol from  
898 open biomass burning smoke in aircraft and laboratory studies, *Atmos. Chem. Phys.*, 11(23),  
899 12049–12064 [online] Available from:  
900 <https://www.atmos-chem-phys.net/11/12049/2011/acp-11-12049-2011.pdf>, 2011.

901 DeCarlo, P. F., Kimmel, J. R., Trimborn, A., Northway, M. J., Jayne, J. T., Aiken, A. C., Gonin,  
902 M., Fuhrer, K., Horvath, T., Docherty, K. S., Worsnop, D. R. and Jimenez, J. L.:  
903 Field-deployable, high-resolution, time-of-flight aerosol mass spectrometer, *Anal. Chem.*,  
904 78(24), 8281–8289, doi:10.1021/ac061249n, 2006.

905 DeCarlo, P. F., Dunlea, E. J., Kimmel, J. R., Aiken, A. C., Sueper, D., Crounse, J., Wennberg, P.  
906 O., Emmons, L., Shinzuka, Y., Clarke, A. and Others: Fast airborne aerosol size and chemistry  
907 measurements above Mexico City and Central Mexico during the MILAGRO campaign, 1foldr  
908 Import 2019-10-08 Batch 1 [online] Available from:  
909 <https://oaktrust.library.tamu.edu/bitstream/handle/1969.1/178622/document-2.pdf?sequence=2>,  
910 2008.

911 Dentener, F. J. and Crutzen, P. J.: A three-dimensional model of the global ammonia cycle, *J.*  
912 *Atmos. Chem.*, 19(4), 331–369, doi:10.1007/BF00694492, 1994.

913 Docherty, K. S., Lewandowski, M. and Jimenez, J. L.: Effect of Vaporizer Temperature on  
914 Ambient Non-Refractory Submicron Aerosol Composition and Mass Spectra Measured by the  
915 Aerosol Mass Spectrometer, *Aerosol Sci. Technol.*, 49(7), 485–494,  
916 doi:10.1080/02786826.2015.1042100, 2015.

917 Dockery, D. W., Cunningham, J., Damokosh, A. I., Neas, L. M., Spengler, J. D., Koutrakis, P.,  
918 Ware, J. H., Raizenne, M. and Speizer, F. E.: Health effects of acid aerosols on North American  
919 children: respiratory symptoms, *Environ. Health Perspect.*, 104(5), 500–505,  
920 doi:10.1289/ehp.96104500, 1996.

921 Dovrou, E., Lim, C. Y., Canagaratna, M. R., Kroll, J. H., Worsnop, D. R. and Keutsch, F. N.:  
922 Measurement techniques for identifying and quantifying hydroxymethanesulfonate (HMS) in an  
923 aqueous matrix and particulate matter using aerosol mass spectrometry and ion chromatography,  
924 *Atmospheric Measurement Techniques*, 12(10), 5303–5315, doi:10.5194/amt-12-5303-2019,

925 2019.

926 Dunlea, E. J., DeCarlo, P. F., Aiken, A. C., Kimmel, J. R., Peltier, R. E., Weber, R. J., Tomlinson,  
927 J., Collins, D. R., Shinozuka, Y., McNaughton, C. S. and Others: Evolution of Asian aerosols  
928 during transpacific transport in INTEX-B, *Atmos. Chem. Phys.*, 9(19), 7257–7287 [online]  
929 Available from: <https://www.atmos-chem-phys.net/9/7257/2009/acp-9-7257-2009.pdf>, 2009.

930 Facchini, M. C., Decesari, S., Rinaldi, M., Carbone, C., Finessi, E., Mircea, M., Fuzzi, S.,  
931 Moretti, F., Tagliavini, E., Ceburnis, D. and O'Dowd, C. D.: Important source of marine  
932 secondary organic aerosol from biogenic amines, *Environ. Sci. Technol.*, 42(24), 9116–9121,  
933 doi:10.1021/es8018385, 2008.

934 Farmer, D. K., Matsunaga, A., Docherty, K. S., Surratt, J. D., Seinfeld, J. H., Ziemann, P. J. and  
935 Jimenez, J. L.: Response of an aerosol mass spectrometer to organonitrates and organosulfates  
936 and implications for atmospheric chemistry, *Proc. Natl. Acad. Sci. U. S. A.*, 107(15), 6670–6675,  
937 doi:10.1073/pnas.0912340107, 2010.

938 Fountoukis, C. and Nenes, A.: ISORROPIA II: a computationally efficient thermodynamic  
939 equilibrium model for  $K^+$ – $Ca^{2+}$ – $Mg^{2+}$ – $NH_4^+$ – $Na^+$ – $SO_4^{2-}$ – $NO_3^-$ – $Cl^-$ – $H_2O$  aero, *Atmos. Chem.*  
940 *Phys.*, 7(17), 4639–4659, doi:10.5194/acp-7-4639-2007, 2007.

941 Friese, E. and Ebel, A.: Temperature Dependent Thermodynamic Model of the System  $H-NH_4$   
942  $-Na-SO_4-NO_3-Cl-H_2O$ , *The Journal of Physical Chemistry A*, 114(43), 11595–11631,  
943 doi:10.1021/jp101041j, 2010.

944 Frossard, A. a., Russell, L. M., Burrows, S. M., Elliott, S. M., Bates, T. S. and Quinn, P. K.:  
945 Sources and Composition of Submicron Organic Mass in Marine Aerosol Particles, *J. Geophys.*  
946 *Res. D: Atmos.*, doi:10.1002/2014JD021913, 2014.

947 Froyd, K. D., Murphy, D. M., Sanford, T. J., Thomson, D. S., Wilson, J. C., Pfister, L. and Lait,  
948 L.: Aerosol composition of the tropical upper troposphere, *Atmos. Chem. Phys.*, 9(13),  
949 4363–4385, doi:10.5194/acp-9-4363-2009, 2009.

950 Froyd, K. D., Murphy, D. M., Brock, C. A., Campuzano-Jost, P., Dibb, J. E., Jimenez, J.-L.,  
951 Kupc, A., Middlebrook, A. M., Schill, G. P., Thornhill, K. L., Williamson, C. J., Wilson, J. C.  
952 and Ziemba, L. D.: A new method to quantify mineral dust and other aerosol species from  
953 aircraft platforms using single-particle mass spectrometry, *Atmospheric Measurement*  
954 *Techniques*, 12(11), 6209–6239, doi:10.5194/amt-12-6209-2019, 2019.

955 Fry, J. L., Draper, D. C., Zarzana, K. J., Campuzano-Jost, P., Day, D. A., Jimenez, J. L., Brown,  
956 S. S., Cohen, R. C., Kaser, L., Hansel, A., Cappellin, L., Karl, T., Hodzic Roux, A., Turnipseed,  
957 A., Cantrell, C., Lefer, B. L. and Grossberg, N.: Observations of gas- and aerosol-phase organic  
958 nitrates at BEACHON-RoMBAS 2011, *Atmospheric Chemistry and Physics*, 13(17),  
959 8585–8605, doi:10.5194/acp-13-8585-2013, 2013.

960 Gaston, C. J., Riedel, T. P., Zhang, Z., Gold, A., Surratt, J. D. and Thornton, J. A.: Reactive  
961 Uptake of an Isoprene-Derived Epoxydiol to Submicron Aerosol Particles, ,

962 doi:10.1021/es5034266, 2014.

963 Gelaro, R., McCarty, W., Suárez, M. J., Todling, R., Molod, A., Takacs, L., Randles, C. A.,  
964 Darmenov, A., Bosilovich, M. G., Reichle, R., Wargan, K., Coy, L., Cullather, R., Draper, C.,  
965 Akella, S., Buchard, V., Conaty, A., da Silva, A. M., Gu, W., Kim, G.-K., Koster, R., Lucchesi,  
966 R., Merkova, D., Nielsen, J. E., Partyka, G., Pawson, S., Putman, W., Rienecker, M., Schubert, S.  
967 D., Sienkiewicz, M. and Zhao, B.: The Modern-Era Retrospective Analysis for Research and  
968 Applications, Version 2 (MERRA-2), *J. Clim.*, 30(14), 5419–5454,  
969 doi:10.1175/JCLI-D-16-0758.1, 2017.

970 Ge, X., Shaw, S. L. and Zhang, Q.: Toward Understanding Amines and Their Degradation  
971 Products from Postcombustion CO<sub>2</sub> Capture Processes with Aerosol Mass Spectrometry,  
972 *Environ. Sci. Technol.* [online] Available from: <http://pubs.acs.org/doi/abs/10.1021/es4056966>,  
973 2014.

974 Gibb, S. W., Mantoura, R. F. C. and Liss, P. S.: Ocean-atmosphere exchange and atmospheric  
975 speciation of ammonia and methylamines in the region of the NW Arabian Sea, *Global*  
976 *Biogeochemical Cycles*, 13(1), 161–178, doi:10.1029/98gb00743, 1999.

977 Giglio, L., Randerson, J. T. and van der Werf, G. R.: Analysis of daily, monthly, and annual  
978 burned area using the fourth-generation global fire emissions database (GFED4), *Journal of*  
979 *Geophysical Research: Biogeosciences*, 118(1), 317–328 [online] Available from:  
980 <https://agupubs.onlinelibrary.wiley.com/doi/abs/10.1002/jgrg.20042>, 2013.

981 Guo, H., Xu, L., Bougiatioti, A., Cerully, K. M., Capps, S. L., Hite, J. R., Jr, Carlton, A. G., Lee,  
982 S.-H., Bergin, M. H., Ng, N. L. and Others: Fine-particle water and pH in the southeastern  
983 United States, *Atmospheric Chemistry & Physics*, 15(9) [online] Available from:  
984 [https://www.researchgate.net/profile/Kate\\_Cerully/publication/276206260\\_Fine-particle\\_water\\_](https://www.researchgate.net/profile/Kate_Cerully/publication/276206260_Fine-particle_water_and_pH_in_the_southeastern_United_States/links/55f6fc8508aeba1d9eee4213.pdf)  
985 [and\\_pH\\_in\\_the\\_southeastern\\_United\\_States/links/55f6fc8508aeba1d9eee4213.pdf](https://www.researchgate.net/profile/Kate_Cerully/publication/276206260_Fine-particle_water_and_pH_in_the_southeastern_United_States/links/55f6fc8508aeba1d9eee4213.pdf), 2015.

986 Guo, H., Sullivan, A. P., Campuzano-Jost, P., Schroder, J. C., Lopez-Hilfiker, F. D., Dibb, J. E.,  
987 Jimenez, J. L., Thornton, J. A., Brown, S. S., Nenes, A. and Others: Fine particle pH and the  
988 partitioning of nitric acid during winter in the northeastern United States, *J. Geophys. Res. D:*  
989 *Atmos.*, 121(17), 10–355 [online] Available from:  
990 <https://onlinelibrary.wiley.com/doi/pdf/10.1002/2016JD025311>, 2016.

991 Guo, H., Liu, J., Froyd, K. D., Roberts, J. M., Veres, P. R., Hayes, P. L., Jimenez, J. L., Nenes, A.  
992 and Weber, R. J.: Fine particle pH and gas–particle phase partitioning of inorganic species in  
993 Pasadena, California, during the 2010 CalNex campaign, *Atmospheric Chemistry and Physics*,  
994 17(9), 5703–5719, doi:10.5194/acp-17-5703-2017, 2017.

995 Guo, H., Campuzano-Jost, P., Nault, B. A., Day, D. A., Schroder, J. C., Dibb, J. E., Dollner, M.,  
996 Weinzierl, B. and Jimenez, J. L.: The Importance of Size Ranges in Aerosol Instrument  
997 Intercomparisons: A Case Study for the ATom Mission, , doi:10.5194/amt-2020-224, 2020.

998 Hennigan, C. J., Sullivan, A. P., Fountoukis, C. I., Nenes, A., Hecobian, A., Vargas, O., Hanks,

999 A. T. C., Huey, L. G., Lefer, B. L., Russell, A. G. and Others: On the volatility and production  
1000 mechanisms of newly formed nitrate and water soluble organic aerosol in Mexico City, [online]  
1001 Available from: <https://hal.archives-ouvertes.fr/hal-00304021/>, 2008.

1002 Hennigan, C. J., Izumi, J., Sullivan, A. P., Weber, R. J. and Nenes, A.: A critical evaluation of  
1003 proxy methods used to estimate the acidity of atmospheric particles, *Atmos. Chem. Phys.*, 15(5),  
1004 2775 [online] Available from:  
1005 <https://pdfs.semanticscholar.org/18b0/f81231da34dbf1e29d753ae7c5e111cbd7fb.pdf>, 2015.

1006 Hodshire, A. L., Campuzano-Jost, P., Kodros, J. K., Croft, B., Nault, B. A., Schroder, J. C.,  
1007 Jimenez, J. L. and Pierce, J. R.: The potential role of methanesulfonic acid (MSA) in aerosol  
1008 formation and growth and the associated radiative forcings, *Atmos. Chem. Phys.*, 19(5),  
1009 3137–3160, doi:10.5194/acp-19-3137-2019, 2019.

1010 Hodzic, A., Campuzano-Jost, P., Bian, H., Chin, M., Colarco, P. R., Day, D. A., Froyd, K. D.,  
1011 Heinold, B., Jo, D. S., Katich, J. M. and Others: Characterization of Organic Aerosol across the  
1012 Global Remote Troposphere: A comparison of ATom measurements and global chemistry  
1013 models, *Atmos. Chem. Phys.*, 2020.

1014 Hoesly, R. M., Smith, S. J., Feng, L., Klimont, Z., Janssens-Maenhout, G., Pitkanen, T., Seibert,  
1015 J. J., Vu, L., Andres, R. J., Bolt, R. M. and Others: Historical (1750--2014) anthropogenic  
1016 emissions of reactive gases and aerosols from the Community Emissions Data System (CEDS),  
1017 Geoscientific Model Development (Online), 11(PNNL-SA-123932) [online] Available from:  
1018 <https://www.osti.gov/biblio/1421326>, 2018.

1019 Huang, S., Poulain, L., van Pinxteren, D., van Pinxteren, M., Wu, Z., Herrmann, H. and  
1020 Wiedensohler, A.: Latitudinal and Seasonal Distribution of Particulate MSA over the Atlantic  
1021 using a Validated Quantification Method with HR-ToF-AMS, *Environ. Sci. Technol.*, 51(1),  
1022 418–426, doi:10.1021/acs.est.6b03186, 2017.

1023 Huffman, J. A., Jayne, J. T., Drewnick, F., Aiken, A. C., Onasch, T., Worsnop, D. R. and  
1024 Jimenez, J. L.: Design, Modeling, Optimization, and Experimental Tests of a Particle Beam  
1025 Width Probe for the Aerodyne Aerosol Mass Spectrometer, *Aerosol Sci. Technol.*, 39(12),  
1026 1143–1163, doi:10.1080/02786820500423782, 2005.

1027 Hu, W., Campuzano-Jost, P., Day, D. A., Croteau, P., Canagaratna, M. R., Jayne, J. T., Worsnop,  
1028 D. R. and Jimenez, J. L.: Evaluation of the new capture vaporizer for aerosol mass spectrometers  
1029 (AMS) through field studies of inorganic species, *Aerosol Sci. Technol.*, 51(6), 735–754,  
1030 doi:10.1080/02786826.2017.1296104, 2017a.

1031 Hu, W., Campuzano-Jost, P., Day, D. A., Croteau, P., Canagaratna, M. R., Jayne, J. T., Worsnop,  
1032 D. R. and Jimenez, J. L.: Evaluation of the new capture vapourizer for aerosol mass  
1033 spectrometers (AMS) through laboratory studies of inorganic species, *Atmospheric Measurement*  
1034 *Techniques*, 10(8), doi:10.5194/amt-10-2897-2017, 2017b.

1035 Hu, W., Campuzano-Jost, P., Day, D. A., Nault, B., Park, T., Lee, T., Pajunoja, A., Virtanen, A.,

1036 Croteau, P. L., Canagaratna, M. R., Jayne, J. T., Worsnop, D. R. and Jimenez, J. L.: Ambient  
1037 quantification and size distributions for organic aerosol (OA) in aerosol mass spectrometer  
1038 (AMS) instruments with the new capture vaporizer (CV), *ACS Earth and Space Chemistry*,  
1039 doi:10.1021/acsearthspacechem.9b00310, 2020.

1040 Hu, W. W., Campuzano-Jost, P., Palm, B. B., Day, D. A., Ortega, A. M., Hayes, P. L., Krechmer,  
1041 J. E., Chen, Q., Kuwata, M., Liu, Y. J. and Others: Characterization of a real-time tracer for  
1042 isoprene epoxydiols-derived secondary organic aerosol (IEPOX-SOA) from aerosol mass  
1043 spectrometer measurements, *Atmos. Chem. Phys.*, 15(20), 11807–11833 [online] Available from:  
1044 <https://www.atmos-chem-phys.net/15/11807/2015/acp-15-11807-2015.html>, 2015.

1045 IPCC: IPCC 2013: Climate Change 2013: The Physical Science Basis. Contribution of Working  
1046 Group I to the Fifth Assessment Report of the Intergovernmental Panel on Climate Change,  
1047 edited by T. F. Stocker, D. Qin, G. K. Plattner, M. Tignor, S. K. Allen, V. Bex, and P. M.  
1048 Midgley, Cambridge University Press, Cambridge, United Kingdom and New York, NY, USA.,  
1049 2013.

1050 Jaeglé, L., Shah, V., Thornton, J. A., Lopez-Hilfiker, F. D., Lee, B. H., McDuffie, E. E., Fibiger,  
1051 D., Brown, S. S., Veres, P., Sparks, T., Ebben, C., Wooldridge, P. J., Kenagy, H. S., Cohen, R. C.,  
1052 Weinheimer, A. J., Campos, T. L., Montzka, D. D., Digangi, J. P., Wolfe, G. M., Hanisco, T.,  
1053 Schroder, J. C., Campuzano-Jost, P., Day, D. A., Jimenez, J. L., Sullivan, A. P., Guo, H. and  
1054 Weber, R. J.: Nitrogen Oxides Emissions, Chemistry, Deposition, and Export Over the  
1055 Northeast United States During the WINTER Aircraft Campaign, *J. Geophys. Res. D: Atmos.*,  
1056 (2), 368–393, doi:10.1029/2018JD029133, 2018.

1057 Jang, M., Czoschke, N. M., Lee, S. and Kamens, R. M.: Heterogeneous atmospheric aerosol  
1058 production by acid-catalyzed particle-phase reactions, *Science*, 298(5594), 814–817,  
1059 doi:10.1126/science.1075798, 2002.

1060 Jayne, J. T., Leard, D. C., Zhang, X., Davidovits, P., Smith, K. A., Kolb, C. E. and Worsnop, D.  
1061 R.: Development of an Aerosol Mass Spectrometer for Size and Composition Analysis of  
1062 Submicron Particles, *Aerosol Sci. Technol.*, 33(1-2), 49–70, doi:10.1080/027868200410840,  
1063 2000.

1064 Jimenez, J. L., Jayne, J. T., Shi, Q., Kolb, C. E., Worsnop, D. R., Yourshaw, I., Seinfeld, J. H.,  
1065 Flagan, R. C., Zhang, X. F., Smith, K. A., Morris, J. W. and Davidovits, P.: Ambient aerosol  
1066 sampling using the Aerodyne Aerosol Mass Spectrometer, *J. Geophys. Res.*, 108(D7),  
1067 8425–8425, doi:10.1029/2001JD001213, 2003.

1068 Jimenez, J. L., Canagaratna, M. R., Donahue, N. M., Prevot, A. S. H., Zhang, Q., Kroll, J. H.,  
1069 DeCarlo, P. F., Allan, J. D., Coe, H., Ng, N. L., Aiken, A. C., Docherty, K. S., Ulbrich, I. M.,  
1070 Grieshop, A. P., Robinson, A. L., Duplissy, J., Smith, J. D., Wilson, K. R., Lanz, V. A., Hueglin,  
1071 C., Sun, Y. L., Tian, J., Laaksonen, A., Raatikainen, T., Rautiainen, J., Vaattovaara, P., Ehn, M.,  
1072 Kulmala, M., Tomlinson, J. M., Collins, D. R., Cubison, M. J., Dunlea, E. J., Huffman, J. A.,  
1073 Onasch, T. B., Alfarra, M. R., Williams, P. I., Bower, K., Kondo, Y., Schneider, J., Drewnick, F.,  
1074 Borrmann, S., Weimer, S., Demerjian, K., Salcedo, D., Cottrell, L., Griffin, R., Takami, A.,

1075 Miyoshi, T., Hatakeyama, S., Shimono, A., Sun, J. Y., Zhang, Y. M., Dzepina, K., Kimmel, J. R.,  
1076 Sueper, D., Jayne, J. T., Herndon, S. C., Trimborn, A. M., Williams, L. R., Wood, E. C.,  
1077 Middlebrook, A. M., Kolb, C. E., Baltensperger, U. and Worsnop, D. R.: Evolution of organic  
1078 aerosols in the atmosphere, *Science*, 326(5959), 1525–1529, doi:10.1126/science.1180353, 2009.

1079 Jo, D. S., Hodzic, A., Emmons, L. K., Marais, E. A., Peng, Z., Nault, B. A., Hu, W.,  
1080 Campuzano-Jost, P. and Jimenez, J. L.: A simplified parameterization of  
1081 isoprene-epoxydiol-derived secondary organic aerosol (IEPOX-SOA) for global chemistry and  
1082 climate models: a case study with GEOS-Chem v11-02-rc, *Geoscientific Model Development*,  
1083 12(7), 2983–3000, doi:10.5194/gmd-12-2983-2019, 2019.

1084 Johnson, K. S., Laskin, A., Jimenez, J. L., Shutthanandan, V., Molina, L. T., Salcedo, D.,  
1085 Dzepina, K. and Molina, M. J.: Comparative analysis of urban atmospheric aerosol by  
1086 particle-induced X-ray emission (PIXE), proton elastic scattering analysis (PESA), and aerosol  
1087 mass spectrometry (AMS), *Environ. Sci. Technol.*, 42(17), 6619–6624, doi:10.1021/es800393e,  
1088 2008.

1089 Kang, H., Day, D. A., Krechmer, J. E., Ayres, B. R., Keehan, N. I., Thompson, S. L., Hu, W.,  
1090 Campuzano-Jost, P., Schroder, J. C., Stark, H., Ranney, A., Ziemann, P., Zarzana, K. J., Wild, R.  
1091 J., Dubé, W., Brown, S. S., Fry, J. and Jimenez, J. L.: A33E-0280: Secondary organic aerosol  
1092 mass yields from the dark NO<sub>3</sub> oxidation of  $\alpha$ -pinene and-carene: effect of RO<sub>2</sub> radical fate, in  
1093 American Geophysical Union Fall Meeting., San Francisco, CA, USA, 12-16 December 2016.

1094 Keene, W. C.: Variation of marine aerosol acidity with particle size, *Geophys. Res. Lett.*, 29(7),  
1095 20,565, doi:10.1029/2001GL013881, 2002.

1096 Lambert, J. B.: *Organic structural spectroscopy*, Pearson College Division., 1998.

1097 Lee, B. H., Lopez-Hilfiker, F. D., Mohr, C., Kurtén, T., Worsnop, D. R. and Thornton, J. a.: An  
1098 iodide-adduct high-resolution time-of-flight chemical-ionization mass spectrometer: application  
1099 to atmospheric inorganic and organic compounds, *Environ. Sci. Technol.*, 48(11), 6309–6317,  
1100 doi:10.1021/es500362a, 2014.

1101 Lee, B. H., Lopez-Hilfiker, F. D., Veres, P. R., McDuffie, E. E., Fibiger, D. L., Sparks, T. L.,  
1102 Ebben, C. J., Green, J. R., Schroder, J. C., Campuzano-Jost, P. and Others: Flight deployment of  
1103 a high-resolution time-of-flight chemical ionization mass spectrometer: Observations of reactive  
1104 halogen and nitrogen oxide species, *J. Geophys. Res. D: Atmos.*, 123(14), 7670–7686 [online]  
1105 Available from:  
1106 [https://agupubs.onlinelibrary.wiley.com/doi/abs/10.1029/2017JD028082@10.1002/\(ISSN\)2169-](https://agupubs.onlinelibrary.wiley.com/doi/abs/10.1029/2017JD028082@10.1002/(ISSN)2169-1107)  
1107 8996.WINTER1, 2018.

1108 Lee, T., Sullivan, A. P., Mack, L., Jimenez, J. L., Kreidenweis, S. M., Onasch, T. B., Worsnop, D.  
1109 R., Malm, W., Wold, C. E., Hao, W. M. and Collett, J. L.: Chemical Smoke Marker Emissions  
1110 During Flaming and Smoldering Phases of Laboratory Open Burning of Wildland Fuels, *Aerosol*  
1111 *Sci. Technol.*, 44(9), i–v, doi:10.1080/02786826.2010.499884, 2010.

1112 Liao, J., Froyd, K. D., Murphy, D. M., Keutsch, F. N., Yu, G., Wennberg, P. O., Clair, J. M. S.,  
1113 Crounse, J. D., Wisthaler, A., Mikoviny, T. and Others: Airborne measurements of  
1114 organosulfates over the continental US, *J. Geophys. Res. D: Atmos.*, 120(7), 2990–3005 [online]  
1115 Available from:  
1116 <https://agupubs.onlinelibrary.wiley.com/doi/abs/10.1002/2014JD022378>  
1117 [%4010.1002/%28ISSN](https://doi.org/10.1002/2014JD022378)  
[%292169-8996.SEAFOURC1](https://doi.org/10.1002/2014JD022378), 2015.

1118 Li, G., Bei, N., Cao, J., Huang, R., Wu, J., Feng, T., Wang, Y., Liu, S., Zhang, Q., Tie, X. and  
1119 Molina, L. T.: A possible pathway for rapid growth of sulfate during haze days in China, ,  
1120 3301–3316 [online] Available from: <https://dspace.mit.edu/handle/1721.1/109728?show=full>  
1121 (Accessed 2 August 2019), 2017.

1122 Lighty, J. S., Veranth, J. M. and Sarofim, A. F.: Combustion aerosols: factors governing their size  
1123 and composition and implications to human health, *J. Air Waste Manag. Assoc.*, 50(9),  
1124 1565–618; discussion 1619–22 [online] Available from:  
1125 <https://www.ncbi.nlm.nih.gov/pubmed/11055157>, 2000.

1126 Liu, P., Ziemann, P. J., Kittelson, D. B. and McMurry, P. H.: Generating Particle Beams of  
1127 Controlled Dimensions and Divergence: II. Experimental Evaluation of Particle Motion in  
1128 Aerodynamic Lenses and Nozzle Expansions, *Aerosol Sci. Technol.*, 22(3), 314–324,  
1129 doi:10.1080/02786829408959749, 1995.

1130 Liu, X., Day, D. A., Krechmer, J. E., Brown, W., Peng, Z., Ziemann, P. J. and Jimenez, J. L.:  
1131 Direct measurements of semi-volatile organic compound dynamics show near-unity mass  
1132 accommodation coefficients for diverse aerosols, *Communications Chemistry*, 2(1), 1–9,  
1133 doi:10.1038/s42004-019-0200-x, 2019.

1134 Lohmann, U., Broekhuizen, K., Leaitch, R., Shantz, N. and Abbatt, J.: How efficient is cloud  
1135 droplet formation of organic aerosols?, *Geophys. Res. Lett.*, 31(5), 2004.

1136 Losey, D. J., Ott, E.-J. E. and Freedman, M. A.: Effects of High Acidity on Phase Transitions of  
1137 an Organic Aerosol, *J. Phys. Chem. A*, 122(15), 3819–3828, doi:10.1021/acs.jpca.8b00399,  
1138 2018.

1139 Massucci, M., Clegg, S. L. and Brimblecombe, P.: Equilibrium Partial Pressures,  
1140 Thermodynamic Properties of Aqueous and Solid Phases, and Cl<sub>2</sub> Production from Aqueous  
1141 HCl and HNO<sub>3</sub> and Their Mixtures, *J. Phys. Chem. A*, 103(21), 4209–4226,  
1142 doi:10.1021/jp9847179, 1999.

1143 Matthew, B. M., Middlebrook, A. M. and Onasch, T. B.: Collection Efficiencies in an Aerodyne  
1144 Aerosol Mass Spectrometer as a Function of Particle Phase for Laboratory Generated Aerosols,  
1145 *Aerosol Sci. Technol.*, 42(11), 884–898, doi:10.1080/02786820802356797, 2008.

1146 Meskhidze, N., Chameides, W. L., Nenes, A. and Chen, G.: Iron mobilization in mineral dust:  
1147 Can anthropogenic SO<sub>2</sub> emissions affect ocean productivity?, *Geophys. Res. Lett.*, 30(21)  
1148 [online] Available from:

- 1149 <https://agupubs.onlinelibrary.wiley.com/doi/abs/10.1029/2003GL018035>, 2003.
- 1150 Middlebrook, A. M., Bahreini, R., Jimenez, J. L. and Canagaratna, M. R.: Evaluation of  
1151 Composition-Dependent Collection Efficiencies for the Aerodyne Aerosol Mass Spectrometer  
1152 using Field Data, *Aerosol Sci. Technol.*, 46(3), 258–271, doi:10.1080/02786826.2011.620041,  
1153 2012.
- 1154 Müller, C., Iinuma, Y., Karstensen, J., Van Pinxteren, D., Lehmann, S., Gnauk, T. and Herrmann,  
1155 H.: Seasonal variation of aliphatic amines in marine sub-micrometer particles at the Cape Verde  
1156 islands, [online] Available from: <https://oar.tib.eu/jspui/handle/123456789/261>, 2009.
- 1157 Murphy, S. M., Sorooshian, A., Kroll, J. H., Ng, N. L., Chhabra, P., Tong, C., Surratt, J. D.,  
1158 Knipping, E., Flagan, R. C. and Seinfeld, J. H.: Secondary aerosol formation from atmospheric  
1159 reactions of aliphatic amines, *Atmospheric Chemistry and Physics Discussions*, 7(1), 289–349,  
1160 doi:10.5194/acpd-7-289-2007, 2007.
- 1161 Nault, B. A., Campuzano-Jost, P., Day, D. A., Schroder, J. C., Anderson, B., Beyersdorf, A. J.,  
1162 Blake, D. R., Brune, W. H., Choi, Y., Corr, C. A., Gouw, J. A. de, Dibb, J., DiGangi, J. P., Diskin,  
1163 G. S., Fried, A., Huey, L. G., Kim, M. J., Knote, C. J., Lamb, K. D., Lee, T., Park, T., Pusede, S.  
1164 E., Scheuer, E., Thornhill, K. L., Woo, J.-H. and Jimenez, J. L.: Secondary organic aerosol  
1165 production from local emissions dominates the organic aerosol budget over Seoul, South Korea,  
1166 during KORUS-AQ, *Atmos. Chem. Phys.*, 18(24), 17769–17800,  
1167 doi:10.5194/acp-18-17769-2018, 2018.
- 1168 Nault, B. A., Campuzano-Jost, P., Jo, D., Day, D., Bahreini, R., Bian, H., Chin, M., Clegg, S.,  
1169 Colarco, P., Kodros, J., Lopez-Hilfiker, F., Marais, E., Middlebrook, A., Neuman, A., Nowak, J.,  
1170 Pierce, J., Thornton, J., Tsigaridis, K., Jimenez, J. and ATom Science Team: Global Survey of  
1171 Aerosol Acidity from Polluted to Remote Locations: Measurements and Comparisons with  
1172 Global Models, display, doi:10.5194/egusphere-egu2020-11366, 2020.
- 1173 Nault, B. A., Campuzano-Jost, P., Day, D. A., Jo, D. S., Schroder, J. S., Allen, H. M., Bahreini,  
1174 R., Bian, H., Blake, D. R., Chin, M., Clegg, S. L., Colarco, P. R., Crouse, J. D., Cubison, M. J.,  
1175 DeCarlo, P. F., Dibb, J. E., Diskin, G. S., Hodzic, A., Hu, W., Katich, J., Kim, M. J., Kodros, J.  
1176 K., Kupc, A., Lopez-Hilfiker, F. D., Marais, E. A., Middlebrook, A. M., Neuman, J. A., Nowak,  
1177 J. B., Palm, B. B., Paulot, F., Pierce, J. R., Schill, G. P., Scheuer, E., Thornton, J. A., Tsigaridis,  
1178 K., Wennberg, P. O., Williamson, C. J. and Jimenez, J. L.: Models underestimate the increase of  
1179 acidity with remoteness biasing radiative impact calculations, *Communications Earth &*  
1180 *Environment* [submitted], 2021.
- 1181 Nenes, A., Pandis, S. N. and Pilinis, C.: Continued development and testing of a new  
1182 thermodynamic aerosol module for urban and regional air quality models, *Atmos. Environ.*,  
1183 33(10), 1553–1560, doi:10.1016/S1352-2310(98)00352-5, 1999.
- 1184 Ng, N. L., Herndon, S. C., Trimborn, A., Canagaratna, M. R., Croteau, P. L., Onasch, T. B.,  
1185 Sueper, D., Worsnop, D. R., Zhang, Q., Sun, Y. L. and Jayne, J. T.: An Aerosol Chemical  
1186 Speciation Monitor (ACSM) for Routine Monitoring of the Composition and Mass



1187 Concentrations of Ambient Aerosol, *Aerosol Sci. Technol.*, 45(7), 780–794,  
1188 doi:10.1080/02786826.2011.560211, 2011a.

1189 Ng, N. L., Canagaratna, M. R., Jimenez, J. L., Chhabra, P. S., Seinfeld, J. H. and Worsnop, D. R.:  
1190 Changes in organic aerosol composition with aging inferred from aerosol mass spectra, *Atmos.*  
1191 *Chem. Phys.*, 11(13), 6465 [online] Available from:  
1192 <http://citeseerx.ist.psu.edu/viewdoc/download?doi=10.1.1.388.4858&rep=rep1&type=pdf>,  
1193 2011b.

1194 Ovadnevaite, J., Ceburnis, D., Canagaratna, M., Berresheim, H., Bialek, J., Martucci, G.,  
1195 Worsnop, D. R. and O’Dowd, C.: On the effect of wind speed on submicron sea salt mass  
1196 concentrations and source fluxes, *J. Geophys. Res. D: Atmos.*, 117(D16) [online] Available from:  
1197 <https://agupubs.onlinelibrary.wiley.com/doi/abs/10.1029/2011JD017379>, 2012.

1198 Paulot, F., Jacob, D. J., Johnson, M. T., Bell, T. G., Baker, A. R., Keene, W. C., Lima, I. D.,  
1199 Doney, S. C. and Stock, C. A.: Global oceanic emission of ammonia: Constraints from seawater  
1200 and atmospheric observations, *Global Biogeochem. Cycles*, 29(8), 1165–1178,  
1201 doi:10.1002/2015GB005106, 2015.

1202 Phinney, L., Richard Leitch, W., Lohmann, U., Boudries, H., Worsnop, D. R., Jayne, J. T.,  
1203 Toom-Saunty, D., Wadleigh, M., Sharma, S. and Shantz, N.: Characterization of the aerosol over  
1204 the sub-arctic north east Pacific Ocean, *Deep Sea Res. Part 2 Top. Stud. Oceanogr.*, 53(20),  
1205 2410–2433, doi:10.1016/j.dsr2.2006.05.044, 2006.

1206 van Pinxteren, M., Fiedler, B., van Pinxteren, D., Iinuma, Y., Körtzinger, A. and Herrmann, H.:  
1207 Chemical characterization of sub-micrometer aerosol particles in the tropical Atlantic Ocean:  
1208 marine and biomass burning influences, *J. Atmos. Chem.*, 72(2), 105–125,  
1209 doi:10.1007/s10874-015-9307-3, 2015.

1210 Pye, H. O. T., Liao, H., Wu, S., Mickley, L. J., Jacob, D. J., Henze, D. K. and Seinfeld, J. H.:  
1211 Effect of changes in climate and emissions on future sulfate-nitrate-ammonium aerosol levels in  
1212 the United States, *J. Geophys. Res. D: Atmos.*, 114(D1) [online] Available from:  
1213 <https://agupubs.onlinelibrary.wiley.com/doi/abs/10.1029/2008JD010701>, 2009.

1214 Pye, H. O. T., Nenes, A., Alexander, B., Ault, A. P., Barth, M. C., Clegg, S. L., Collett, J. L., Jr,  
1215 Fahey, K. M., Hennigan, C. J., Herrmann, H. and Others: The Acidity of Atmospheric Particles  
1216 and Clouds, UMBC Faculty Collection [online] Available from:  
1217 <https://www.atmos-chem-phys-discuss.net/acp-2019-889/acp-2019-889.pdf>, 2019.

1218 Quinn, P. K., Charlson, R. J. and Bates, T. S.: Simultaneous observations of ammonia in the  
1219 atmosphere and ocean, *Nature*, 335(6188), 336–338, doi:10.1038/335336a0, 1988.

1220 Quinn, P. K., Bates, T. S., Coffman, D., Onasch, T. B., Worsnop, D., Baynard, T., De Gouw, J.  
1221 A., Goldan, P. D., Kuster, W. C., Williams, E. and Others: Impacts of sources and aging on  
1222 submicrometer aerosol properties in the marine boundary layer across the Gulf of Maine, *J.*  
1223 *Geophys. Res. D: Atmos.*, 111(D23) [online] Available from:

- 1224 <https://agupubs.onlinelibrary.wiley.com/doi/abs/10.1029/2006JD007582>, 2006.
- 1225 Raizenne, M., Neas, L. M., Damokosh, A. I., Dockery, D. W., Spengler, J. D., Koutrakis, P.,  
1226 Ware, J. H. and Speizer, F. E.: Health effects of acid aerosols on North American children:  
1227 pulmonary function, *Environ. Health Perspect.*, 104(5), 506–514, doi:10.1289/ehp.96104506,  
1228 1996.
- 1229 Rindelaub, J. D., Craig, R. L., Nandy, L., Bondy, A. L., Dutcher, C. S., Shepson, P. B. and Ault,  
1230 A. P.: Direct Measurement of pH in Individual Particles via Raman Microspectroscopy and  
1231 Variation in Acidity with Relative Humidity, *J. Phys. Chem. A*, 120(6), 911–917,  
1232 doi:10.1021/acs.jpca.5b12699, 2016.
- 1233 Riva, M., Budisulistiorini, S. H., Chen, Y., Zhang, Z., D’Ambro, E. L., Zhang, X., Gold, A.,  
1234 Turpin, B. J., Thornton, J. A., Canagaratna, M. R. and Surratt, J. D.: Chemical Characterization  
1235 of Secondary Organic Aerosol from Oxidation of Isoprene Hydroxyhydroperoxides, *Environ.*  
1236 *Sci. Technol.*, acs.est.6b02511–acs.est.6b02511, doi:10.1021/acs.est.6b02511, 2016.
- 1237 Riva, M., Chen, Y., Zhang, Y., Lei, Z., Olson, N. E., Boyer, H. C., Narayan, S., Yee, L. D.,  
1238 Green, H. S., Cui, T., Zhang, Z., Baumann, K., Fort, M., Edgerton, E., Budisulistiorini, S. H.,  
1239 Rose, C. A., Ribeiro, I. O., E Oliveira, R. L., Dos Santos, E. O., Machado, C. M. D., Szopa, S.,  
1240 Zhao, Y., Alves, E. G., de Sá, S. S., Hu, W., Knipping, E. M., Shaw, S. L., Duvoisin Junior, S., de  
1241 Souza, R. A. F., Palm, B. B., Jimenez, J.-L., Glasius, M., Goldstein, A. H., Pye, H. O. T., Gold,  
1242 A., Turpin, B. J., Vizuete, W., Martin, S. T., Thornton, J. A., Dutcher, C. S., Ault, A. P. and  
1243 Surratt, J. D.: Increasing Isoprene Epoxydiol-to-Inorganic Sulfate Aerosol Ratio Results in  
1244 Extensive Conversion of Inorganic Sulfate to Organosulfur Forms: Implications for Aerosol  
1245 Physicochemical Properties, *Environ. Sci. Technol.*, 53(15), 8682–8694,  
1246 doi:10.1021/acs.est.9b01019, 2019.
- 1247 Salcedo, D., Onasch, T. B., Aiken, a. C., Williams, L. R., de Foy, B., Cubison, M. J., Worsnop,  
1248 D. R., Molina, L. T. and Jimenez, J. L.: Determination of particulate lead using aerosol mass  
1249 spectrometry: MILAGRO/MCMA-2006 observations, *Atmos. Chem. Phys.*, 10(12), 5371–5389,  
1250 doi:10.5194/acp-10-5371-2010, 2010.
- 1251 Schindler, D. W.: Effects of Acid rain on freshwater ecosystems, *Science*, 239(4836), 149–157,  
1252 doi:10.1126/science.239.4836.149, 1988.
- 1253 Schroder, J. C., Campuzano-Jost, P., Day, D. A., Shah, V., Larson, K., Sommers, J. M., Sullivan,  
1254 A. P., Campos, T., Reeves, J. M., Hills, A., Hornbrook, R. S., Blake, N. J., Scheuer, E., Guo, H.,  
1255 Fibiger, D. L., McDuffie, E. E., Hayes, P. L., Weber, R. J., Dibb, J. E., Apel, E. C., Jaeglé, L.,  
1256 Brown, S. S., Thornton, J. A. and Jimenez, J. L.: Sources and Secondary Production of Organic  
1257 Aerosols in the Northeastern United States during WINTER, *J. Geophys. Res. D: Atmos.*, 42,  
1258 4478, doi:10.1029/2018JD028475, 2018.
- 1259 Seinfeld, J. H. and Pandis, S. N.: *Atmospheric Chemistry and Physics*, 2nd ed., John Wiley &  
1260 Sons, Inc., New York., 2006.

1261 Song, S., Gao, M., Xu, W., Shao, J., Shi, G., Wang, S., Wang, Y., Sun, Y. and McElroy, M. B.:  
1262 Fine-particle pH for Beijing winter haze as inferred from different thermodynamic equilibrium  
1263 models, *Atmos. Chem. Phys.*, 18(10), 7423–7438, doi:10.5194/acp-18-7423-2018, 2018.

1264 Song, S., Gao, M., Xu, W., Sun, Y., Worsnop, D. R., Jayne, J. T., Zhang, Y., Zhu, L., Li, M.,  
1265 Zhou, Z. and Others: Possible heterogeneous chemistry of hydroxymethanesulfonate (HMS) in  
1266 northern China winter haze, *Atmos. Chem. Phys.*, 19(2), 1357–1371 [online] Available from:  
1267 <https://www.atmos-chem-phys.net/19/1357/2019/acp-19-1357-2019.pdf>, 2019.

1268 Sorooshian, A., Padró, L. T., Nenes, A., Feingold, G., McComiskey, A., Hersey, S. P., Gates, H.,  
1269 Jonsson, H. H., Miller, S. D., Stephens, G. L. and Others: On the link between ocean biota  
1270 emissions, aerosol, and maritime clouds: Airborne, ground, and satellite measurements off the  
1271 coast of California, *Global Biogeochem. Cycles*, 23(4) [online] Available from:  
1272 <https://agupubs.onlinelibrary.wiley.com/doi/abs/10.1029/2009GB003464>, 2009.

1273 Sorooshian, A., Crosbie, E., Maudlin, L. C., Youn, J.-S., Wang, Z., Shingler, T., Ortega, A. M.,  
1274 Hersey, S. and Woods, R. K.: Surface and airborne measurements of organosulfur and  
1275 methanesulfonate over the western United States and coastal areas, *J. Geophys. Res. D: Atmos.*,  
1276 120(16), 8535–8548, doi:10.1002/2015JD023822, 2015.

1277 Stith, J. L., Ramanathan, V., Cooper, W. A., Roberts, G. C., DeMott, P. J., Carmichael, G., Hatch,  
1278 C. D., Adhikary, B., Twohy, C. H., Rogers, D. C., Baumgardner, D., Prenni, A. J., Campos, T.,  
1279 Gao, R., Anderson, J. and Feng, Y.: An overview of aircraft observations from the Pacific Dust  
1280 Experiment campaign, *J. Geophys. Res.*, 114(D5), 833, doi:10.1029/2008JD010924, 2009.

1281 Sueper, D.: ToF-AMS Data Analysis Software Webpage, [online] Available from:  
1282 [http://cires1.colorado.edu/jimenez-group/wiki/index.php/ToF-AMS\\_Analysis\\_Software](http://cires1.colorado.edu/jimenez-group/wiki/index.php/ToF-AMS_Analysis_Software)  
1283 (Accessed 4 January 2017), 2018.

1284 Surratt, J. D., Kroll, J. H., Kleindienst, T. E., Edney, E. O., Claeys, M., Sorooshian, A., Ng, N.  
1285 L., Offenberg, J. H., Lewandowski, M., Jaoui, M., Flagan, R. C. and Seinfeld, J. H.: Evidence for  
1286 organosulfates in secondary organic aerosol, *Environ. Sci. Technol.*, 41(2), 517–527,  
1287 doi:10.1021/es062081q, 2007.

1288 Surratt, J. D., Gómez-González, Y., Chan, A. W. H., Vermeylen, R., Shahgholi, M., Kleindienst,  
1289 T. E., Edney, E. O., Offenberg, J. H., Lewandowski, M., Jaoui, M., Maenhaut, W., Claeys, M.,  
1290 Flagan, R. C. and Seinfeld, J. H.: Organosulfate formation in biogenic secondary organic aerosol,  
1291 *J. Phys. Chem. A*, 112(36), 8345–8378, doi:10.1021/jp802310p, 2008.

1292 Thornton, J. A., Jaeglé, L. and McNeill, V. F.: Assessing known pathways for HO<sub>2</sub> loss in  
1293 aqueous atmospheric aerosols: Regional and global impacts on tropospheric oxidants, *J.*  
1294 *Geophys. Res. D: Atmos.*, 113(D5) [online] Available from:  
1295 <https://agupubs.onlinelibrary.wiley.com/doi/abs/10.1029/2007JD009236>, 2008.

1296 Tolocka, M. P. and Turpin, B.: Contribution of organosulfur compounds to organic aerosol mass,  
1297 *Environ. Sci. Technol.*, 46(15), 7978–7983, doi:10.1021/es300651v, 2012.

1298 Toon, O. B., Maring, H., Dibb, J., Ferrare, R., Jacob, D. J., Jensen, E. J., Luo, Z. J., Mace, G. G.,  
1299 Pan, L. L., Pfister, L. and Others: Planning, implementation, and scientific goals of the Studies of  
1300 Emissions and Atmospheric Composition, Clouds and Climate Coupling by Regional Surveys  
1301 (SEAC4RS) field mission, *J. Geophys. Res. D: Atmos.*, 121(9), 4967–5009 [online] Available  
1302 from:  
1303 <https://agupubs.onlinelibrary.wiley.com/doi/abs/10.1002/2015JD024297>%4010.1002/%28ISSN  
1304 %292169-8996.SEAFOURC1, 2016.

1305 Wagner, N. L., Brock, C. A., Angevine, W. M., Beyersdorf, A., Campuzano-Jost, P., Day, D., De  
1306 Gouw, J. A., Diskin, G. S., Gordon, T. D., Graus, M. G. and Others: In situ vertical profiles of  
1307 aerosol extinction, mass, and composition over the southeast United States during SENEX and  
1308 SEAC 4 RS: observations of a modest aerosol enhancement aloft, *Atmos. Chem. Phys.*, 15(12),  
1309 7085–7102 [online] Available from:  
1310 <https://www.atmos-chem-phys.net/15/7085/2015/acp-15-7085-2015.html>, 2015.

1311 Wang, Y., Zhang, Q., Jiang, J., Zhou, W., Wang, B., He, K., Duan, F., Zhang, Q., Philip, S. and  
1312 Xie, Y.: Enhanced sulfate formation during China's severe winter haze episode in January 2013  
1313 missing from current models, *J. Geophys. Res. D: Atmos.*, 119(17), 10–425 [online] Available  
1314 from: <https://agupubs.onlinelibrary.wiley.com/doi/abs/10.1002/2013JD021426>, 2014.

1315 Weber, R. J., Guo, H., Russell, A. G. and Nenes, A.: High aerosol acidity despite declining  
1316 atmospheric sulfate concentrations over the past 15 years, *Nat. Geosci.*, 9, 282,  
1317 doi:10.1038/ngeo2665, 2016.

1318 Wexler, A. S. and Clegg, S. L.: Atmospheric aerosol models for systems including the ions H<sup>+</sup>,  
1319 NH<sub>4</sub><sup>+</sup>, Na<sup>+</sup>, SO<sub>4</sub><sup>2-</sup>, NO<sub>3</sub><sup>-</sup>, Cl<sup>-</sup>, Br<sup>-</sup>, and H<sub>2</sub>O, *J. Geophys. Res. D: Atmos.*, 107(D14), ACH-14  
1320 [online] Available from:  
1321 <https://agupubs.onlinelibrary.wiley.com/doi/abs/10.1029/2001JD000451>, 2002.

1322 Youn, J.-S., Crosbie, E., Maudlin, L. C., Wang, Z. and Sorooshian, A.: Dimethylamine as a major  
1323 alkyl amine species in particles and cloud water: Observations in semi-arid and coastal regions,  
1324 *Atmos. Environ.*, 122, 250–258, doi:10.1016/j.atmosenv.2015.09.061, 2015.

1325 Zhang, Q., Stanier, C. O., Canagaratna, M. R., Jayne, J. T., Worsnop, D. R., Pandis, S. N. and  
1326 Jimenez, J. L.: Insights into the chemistry of new particle formation and growth events in  
1327 Pittsburgh based on aerosol mass spectrometry, *Environ. Sci. Technol.*, 38(18), 4797–4809,  
1328 doi:10.1021/es035417u, 2004a.

1329 Zhang, Q., Jimenez, J. L., Worsnop, D. R. and Canagaratna, M.: A case study of urban particle  
1330 acidity and its influence on secondary organic aerosol, *Environ. Sci. Technol.*, 41(9), 3213–3219,  
1331 doi:10.1021/Es061812j, 2007a.

1332 Zhang, Q., Jimenez, J. L., Canagaratna, M. R., Allan, J. D., Coe, H., Ulbrich, I., Alfarra, M. R.,  
1333 Takami, A., Middlebrook, A. M., Sun, Y. L. and Others: Ubiquity and dominance of oxygenated  
1334 species in organic aerosols in anthropogenically-influenced Northern Hemisphere midlatitudes,  
1335 *Geophys. Res. Lett.*, 34(13) [online] Available from:

1336 <https://agupubs.onlinelibrary.wiley.com/doi/abs/10.1029/2007GL029979%4010.1002/%28ISSN>  
1337 [%291944-8007.GRL40](https://agupubs.onlinelibrary.wiley.com/doi/abs/10.1029/2007GL029979%4010.1002/%28ISSN), 2007b.

1338 Zhang, X., Smith, K. A., Worsnop, D. R., Jimenez, J. L., Jayne, J. T., Kolb, C. E., Morris, J. and  
1339 Davidovits, P.: Numerical Characterization of Particle Beam Collimation: Part II Integrated  
1340 Aerodynamic-Lens–Nozzle System, *Aerosol Sci. Technol.*, 38(6), 619–638,  
1341 doi:10.1080/02786820490479833, 2004b.

1342 Zheng, B., Zhang, Q., Zhang, Y., He, K. B., Wang, K., Zheng, G. J., Duan, F. K., Ma, Y. L. and  
1343 Kimoto, T.: Heterogeneous chemistry: a mechanism missing in current models to explain  
1344 secondary inorganic aerosol formation during the January 2013 haze episode in North China,  
1345 *Atmospheric Chemistry and Physics Discussions*, 14(11), 16731–16776,  
1346 doi:10.5194/acpd-14-16731-2014, 2014.

1347 Zheng, Y., Cheng, X., Liao, K., Li, Y., Li, Y., Huang, R.-J., Hu, W., Liu, Y., Zhu, T., Chen, S. and  
1348 Others: Characterization of Anthropogenic Organic Aerosols by TOF-ACSM with the New  
1349 Capture Vaporizer, *Atmospheric Measurement Techniques* [online] Available from:  
1350 <https://www.atmos-meas-tech-discuss.net/amt-2019-449/amt-2019-449.pdf>, 2020.

1351 Zorn, S. R., Drewnick, F., Schott, M., Hoffmann, T. and Borrmann, S.: Characterization of the  
1352 South Atlantic marine boundary layer aerosol using an aerodyne aerosol mass spectrometer,  
1353 [online] Available from: <https://hal.archives-ouvertes.fr/hal-00304023/>, 2008.